GSMBE GROWTH
ON SiO_2 PATTERNED SUBSTRATES

GSMBE GROWTH AND CHARACTERIZATION OF InGaAs-InP STRUCTURES ON SiO_2 PATTERNED SUBSTRATES

by

SUSAN CAROL NAGY, B. Eng., P.Eng

A Thesis

Submitted to the School of Graduate Studies

in Partial Fulfilment of the Requirements

for the Degree

Master of Engineering

McMaster University

Hamilton, Ontario

MASTER OF ENGINEERING (1995) McMASTER UNIVERSITY

(Engineering Physics) Hamilton, Ontario

TITLE: GSMBE Growth and Characterization of InGaAs-InP Structures on SiO_2 Patterned Substrates.

AUTHOR: Susan Carol Nagy, B.Eng (McMaster University), P.Eng

SUPERVISORS: Professor J.G. Simmons
Professor D.A. Thompson

NUMBER OF PAGES: x, 56

ABSTRACT

Gas source molecular beam epitaxy (GSMBE) has been used to grow InGaAs/InP epitaxial layers in selected areas defined by SiO_2-masked InP substrates, with the goal of obtaining controlled in-plane variations in the bandgap of the InGaAs wells. The ability to alter the bandgap of the semiconductor spatially over the surface in one growth procedure is desirable for integrating laser, waveguide and detector devices.

To form the masked substrates, stripes (ranging in width from 2 μm to 50 μm) were opened up in SiO_2 by standard photolithography. The crystal growths were carried out at various substrate temperatures (ranging from 460 °C to 510 °C) and arsenic fluxes (V/III ratios ranging from 1.2 to 3.4). The properties of the epitaxial layers were investigated by using such analytical techniques as photoluminescence, electroluminescence and transmission electron microscopy (TEM). Photoluminescence measurements performed on waveguide stripes of decreasing width reveal an increasing red-shift of the e1-hh1 transition in InGaAs wells. The maximum red-shift occurred when growing at a high substrate temperature and a low arsenic flux. For example, a decrease in slit width from 50 μm to 10 μm resulted in a 25 meV shift of the photoluminescence peak.

From cross-sectional TEM measurements, the wavelength shift observed can be attributed primarily to an increase in thickness of the InGaAs well, due to incorporation of additional indium and gallium migrating from the material on the masked regions. The interfaces in the centre of the stripe region are defect free; however, stacking faults and thickness variations are evident 1-2 μm from the edges. These results are confirmed by scanning photoluminescence, in which the maximum intensity occurs at the centre of the

stripe and decreases to zero at the edges. Mapping of the peak wavelength across the stripe reveals a diffusion profile, with the edges being additionally red shifted by 10 nm. Reactive ion etching of the edge and the polycrystalline material results in a much improved spectral photoluminescence scan, in both increased intensity of the bandgap peak and elimination of lower energy peaks assumed to be correlated with edge effects.

Finally, a stripe contact light emitting device, with a single 50 Å quantum well InGaAs/InP structure, was fabricated and electrically pumped. The device exhibited spectral peak wavelength shifts between narrow stripes (10 μm) and wide stripes (50 μm) of 22 nm, similar to the value observed by photoluminescence studies.

ACKNOWLEDGEMENTS

I would like to express my appreciation to Dr. Dave Thompson and Dr. John Simmons for their guidance, encouragement and financial support throughout the course of this work. A special thanks to Dr. Brad Robinson for his useful ideas and suggestions. I would like to thank my colleagues at McMaster for their insightful discussions and friendly encouragement. Thanks to Jim Swoger for the use of his apparatus for diode measurements.

I am privileged to have benefited from an international collaborative programme between the Province of Ontario and Region Rhone Alpes in France. The collaboration has allowed me to share knowledge with associates at Ecole Centrale de Lyon. Specifically, special thanks to Farzad Nuban, and his supervisor Dr. S. Krawczyk, for generating numerous scanning photoluminescence spectra from my samples.

I am grateful to the Natural Sciences and Engineering Research Council for providing me with a graduate scholarship.

Finally, I would like to thank my parents and grandma who instilled in me the love of knowledge and the benefits of a good education. To Doug, my greatest supporter and inspiration, thanks for putting up with school life again.

TABLE OF CONTENTS

LIST OF FIGURES

LIST OF TABLES

CHAPTER 1
INTRODUCTION

1.1 MOTIVATION

The ability to control the bandgap energy (E_g) of epitaxially grown structures laterally across a substrate is of significance to integrated optics, particularly to the realization of an optical integrated circuit (OIC). In an OIC, the information is carried by means of a beam of light rather than an electric current. Some advantages of an integrated optical system are reduced weight, increased bandwidth, resistance to electromagnetic interference and low-loss signal transmission [Hunsperger p.7 1991]. There are two basic forms of an OIC. One is the hybrid form, in which devices are fabricated in different materials and then bonded together. The major advantage of hybrid devices are that existing technology can be used to make the individual components; however, the bonds holding the devices together are subject to misalignment or failure. The second form is the monolithic OIC, in which a single substrate material is used for more than one device. To produce an operable monolithic OIC, for example, one which integrates a laser, waveguide and detector, the effective bandgap energies for absorption and emission must vary such that:

$$E_g(\text{waveguide}) > E_g(\text{laser}) > E_g(\text{detector})$$

The major difficulty in fabricating a monolithic OIC has been creating a smooth and high-quality interface between functional elements produced, for example, by subsequent etching and regrowth steps. An emerging technology that represents an attractive alternative is the

technique of selective-area deposition (SAD). In this technique a patterned substrate is used to adjust the epilayer thickness and material composition and, therefore, the bandgap energy, in different areas on the substrate during a single epitaxial growth. When a tapered coupling section exists between functional devices, optical coupling between them may approach 100% since the integrated elements consist of one continuous crystal [Aoki *et al* 1993].

A patterned substrate can be formed by either etching ridges and grooves directly into the substrate or by photolithographically defining windows in a dielectric mask. Selective-area bandgap modification has been achieved on etched substrates by making use of the anisotropy in the migration length of species along different crystallographic directions, to tailor the composition in certain areas. For example, InGaAs layers with areas of increased indium content in grooves can be obtained as a result of preferential indium migration off etched (311)A mesa sidewalls during MBE growth on patterned GaAs substrates [Arent *et al* 1989]. An OIC could be fabricated with a single growth in which the number of active wells in an adjacent device is changed by utilizing the dependence of indium mobility on arsenic overpressure [Pratt *et al* 1994].

Extensive work has also been done using dielectric masks, but mainly on GaAs substrates and using metalorganic chemical vapor deposition (MOCVD) or metalorganic molecular beam epitaxy (MOMBE). Both MOCVD and MOMBE growths have the advantage of total area selectivity, which refers to almost no growth on the mask. Large bandgap shifts of 100 meV between unmasked and masked (5 μm gap, 12 μm mask) regions for multiple quantum well (MQW) InGaAs/InP structures have been reported [Joyner *et al* 1992]. In device applications, Aoki et al used MOCVD to fabricate both a distributed feedback (DFB) laser/modulator structure [Aoki *et al* 1993] as well as a 5-wavelength MQW-DFB laser array with a controllable lasing wavelength range of 10.1 nm for wavelength division multiplexing (WDM) optical communication systems [Aoki *et al* 1995]. MOCVD has also been used to

construct a DFB laser integrated with a waveguide [Tanbun-Ek *et al* 1992]. The difference in the photoluminescence peak between the active region and the passive region was 30 nm, and the estimated absorption loss of the connecting waveguide was 30 cm^{-1}.

In contrast to MOCVD and MOMBE, growth on dielectric patterned substrates by GSMBE results in local epitaxial growth occurring in etched windows, while polycrystalline growth occurs on the dielectric mask. This phase selectivity, where films of different microstructures grow on different substrate materials, is a characteristic of GSMBE and solid-source MBE growth. The polycrystalline regions of GaAs have been reported to have high resistivity (>10^6 Ω cm), resulting in excellent isolation between adjacent single-crystal areas [Cho *et al* 1975]. Area selectivity has been achieved for GaAs at high substrate temperatures (700 °C) [Okamoto 1993]; however, structural deformation of the patterned substrate and cross-impurity diffusion occurs [Shibata *et al* 1993]. Area selectivity has been achieved with lower process temperatures by using migration enhanced epitaxy [Yokoyama *et al* 1993], electron cyclotron resonance GSMBE [Shibata *et al* 1993] and atomic hydrogen irradiation [Kuroda *et al* 1993]. While these techniques suppress the amount of material deposited on the mask, there has been no evidence that these techniques result in larger bandgap energy shifts.

One problem of selective area growth is the enhanced growth which occurs along the perimeter of the openings in which epitaxial growth is taking place. This is referred to as edge growth. The growth rate at the edge is higher than at the centre of the openings of the mask, often with the growth exhibiting (111) faceting for MOCVD, although this is dependent on the growth conditions as well as the geometry and orientation of the substrate and patterned regions. It has been reported that this growth rate enhancement can be minimized for MOMBE by using lower metalorganic and hydride flows, since diffusion is the dominant process at work in the formation of the edge [Cotta *et al* 1993]. The migration length of the

species depends on the arrival rate of the precursor molecules to the substrate, and is determined by the absolute group III and group V flows [Cotta *et al* 1993]. Controlling the edges is important since the removal by wet chemical etching of the edges (1-2 μm) has been shown to significantly improve the electrical characteristics of p-n junctions by decreasing the reverse-bias leakage current by 3 orders of magnitude [Hamm *et al* 1992, Wang *et al* 1991].

1.2 THESIS OBJECTIVE AND OUTLINE

The objective of this work was to achieve in-plane control of the bandgap in the InGaAs/InP materials system grown by GSMBE by utilizing substrates patterned with dielectric masks. The experimental procedures, including preparation of the masked substrate, the epitaxial structure and MBE growth conditions are contained in Chapter 2. Chapter 3 provides an outline of the chacterization methods, specifically photoluminescence and transmission electron microscopy, which were used to measure the bandgap shift, along with the results obtained. The fabrication of an electrically pumped light-emitting device to illustrate the bandgap shift is outlined in Chapter 4. Finally, Chapter 5 summarizes the findings and includes a discussion of future work now possible.

CHAPTER 2
EXPERIMENTAL PROCEDURES

2.1 INTRODUCTION

This chapter examines the MBE growth of undoped InGaAs/InP layers over SiO_2-masked substrates. Epitaxial layers were grown on masked substrates of different stripe widths to examine the morphology and the compositional and thickness changes of the InGaAs well. Section 2.2 outlines the sequence of steps used to produce a SiO_2-masked substrate. The MBE method and surface processes for growth will be presented in section 2.3, with emphasis on GSMBE and the factors which control growth by influencing the kinetics. Based on this discussion, sections 2.4 and 2.5 illustrate the growth structure and conditions used to achieve the peak wavelength shift. Section 2.6 outlines the specific growth procedure used for the experiments, and finally section 2.7 concludes with an image of the wafer after growth.

2.2 SUBSTRATE PATTERNING

The (100) n-type InP substrates used were 15 mm x 15 mm in size, cut from 2" diameter wafers purchased from either Sumitomo (Japan) or Crismatec InPact (France). Figure 2.1 illustrates the specific procedure followed and chemicals used in this work. The wafers are classified as "epiready" by the supplier; however, step 1, which involves a solvent cleaning and chemical etch of the surface, was still performed before depositing the SiO_2.

In step 2, the SiO_2 is deposited onto the InP substrate by a plasma enhanced chemical vapor deposition system. The depositions were typically 1000 Å thick, with the colour being a good indication of the thickness. Next, patterning is performed by lithography, which is the process of transferring shapes on a mask to the surface of a wafer. The general lithographic transfer process, as used in the manufacture of integrated circuits, is well documented [Sze p.267 1983]. The two photomasks used in this thesis are illustrated in appendix 1, figures A.1 and A.2. The masks consist of areas of constant stripe width. One mask covers widths from 5 to 50 µm while the other mask contains stripe widths ranging from 1 to 20 µm. Stripes were oriented in both the [011] or [0$\underline{1}$1] crystallographic direction when aligned on the substrate.

Before the application of the photoresist (PR) in step 3, a HMDS primer (hexamethyldisilazane), is spun on the wafer to improve the PR adhesion by producing an interfacial bonding layer for the PR and by removing residual moisture held at the surface. The liquid photoresist, which is impervious to acid etching but sensitive to UV light, is applied by spinning the wafer at high speeds to produce a uniformly thin layer.

After baking to harden (step 5), the PR is ready for exposure. A Karl Suss mask aligner is used to align a photomask over the wafer and expose the PR to UV light. The mask aligner was used in the high-precision mode, in which a vacuum is pulled between the mask and substrate immediately prior to exposure. The highest possible resolution is obtained, since the gap between the substrate and the mask due to flatness variations is as small as possible. The PR is exposed to UV light, through the transparent areas on the photomask, and becomes soluble in the developer and is washed away (step 8).

A buffered HF solution that does not attack the PR is then used to etch windows in the SiO_2. In step 9, the PR is stripped from the SiO_2. When forming the stripes, the most difficult step, from the point of view of reproducibility, is ensuring that all the SiO_2 and by-

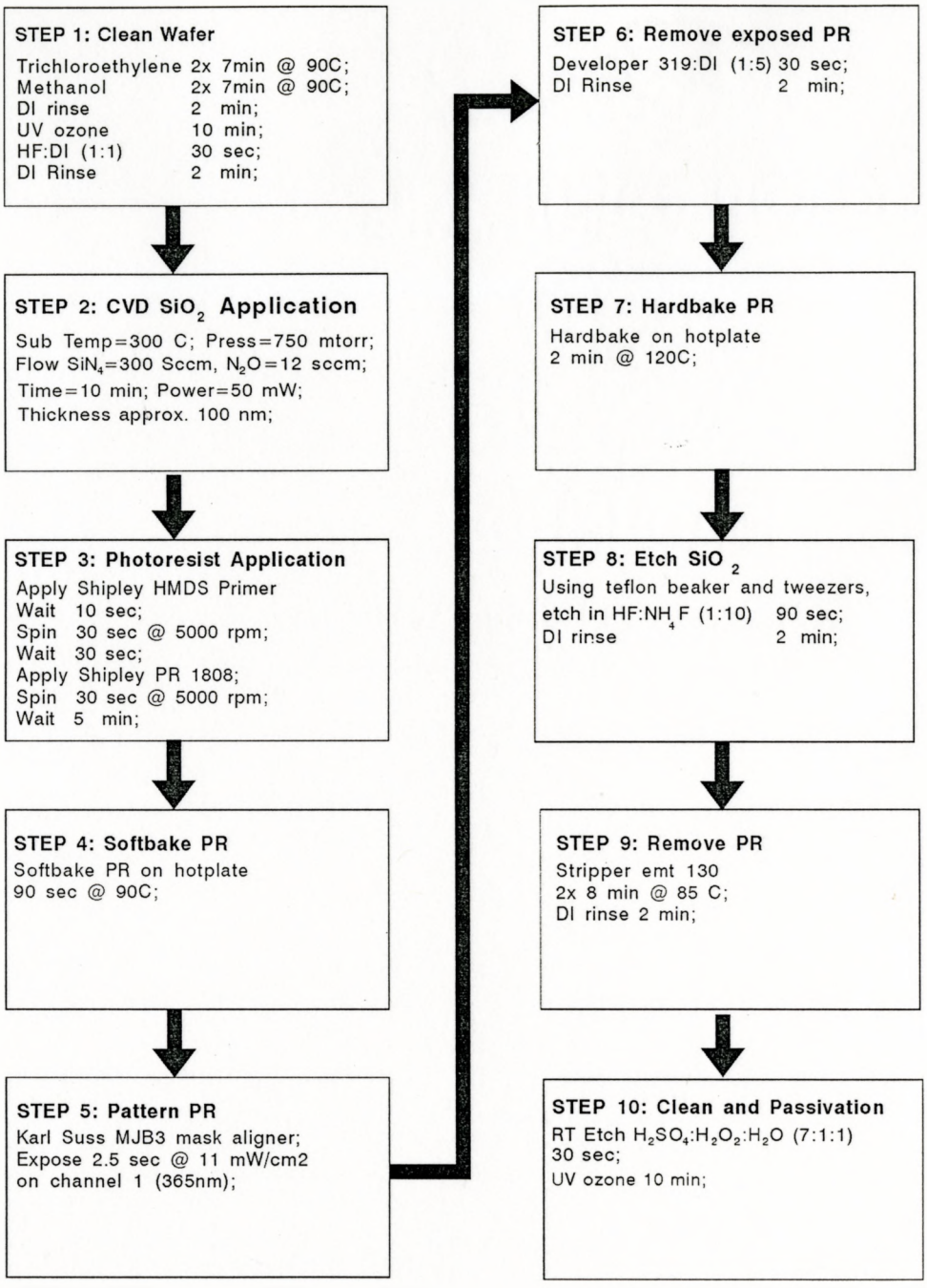

Figure 2.1: *Flowchart illustrating the sequence of processing steps used to pattern the substrate for growth.*

products are removed from the gaps. To ensure cleanliness, the InP substrates are chemically etched in a room temperature mixture of H_2SO_4:H_2O_2:H_2O (7:1:1). Finally, the wafer is prepared for growth by exposing it to UV ozone to remove carbon contamination and increase the native oxide thickness [Hofstra *et al* 1995, Hollinger *et al* 1991]. Passivation in this manner is relatively stable against contamination by laboratory air. Figure 2.2 illustrates a cross-sectional diagram of a patterned substrate ready for growth.

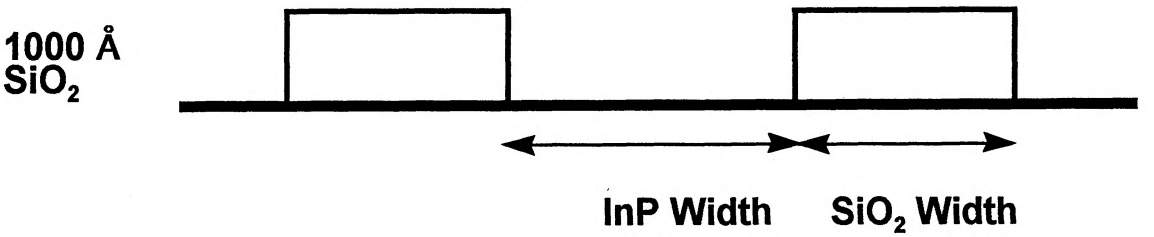

Figure 2.2: *Schematic of the SiO_2-patterned substrate after wet etching. Oxide stripes range in width from 1 to 50 μm while the distance between oxide stripes (InP width) range from 2 to 50 μm.*

2.3 OUTLINE OF GSMBE GROWTH

Molecular beam epitaxy (MBE) is a method of growing high quality epitaxial layers of compound semiconductor films in which atomic or molecular beams containing elements that constitute a particular layer, react with a heated single crystal surface under ultra-high vacuum (UHV) conditions. The name "molecular beam" is derived from the operating condition of molecular flow, implying that the mean free path of the atoms or molecules is larger than the distance from the source to the substrate, therefore negligible interaction occurs between the beams. This is in contrast to other vapor deposition techniques, such as MOCVD, where the transport of reactants in the immediate vicinity of the substrate is essentially characterized by gas phase diffusion.

While a number of different MBE methods exist, all of the growths examined in this thesis were performed using GSMBE. For GSMBE, the atomic beams of the group III elements are generated by evaporation of gallium and indium from effusion cells. The molecular beams of the group V dimeric molecules, As_2 and P_2, are generated by pyrolysis of arsine (AsH_3) and phosphine (PH_3) on a catalytic surface (tantalum or rhenium) in a cracker cell, instead of using elemental sources. For doping the layers n-type and p-type, silicon and beryllium respectively are heated in their own effusion cells. The flux of atoms is controlled by the temperature of the effusion cells and the operation of mechanical shutters positioned in the path of each molecular beam. Multilayer structures are grown by opening and closing the appropriate shutters during layer growth. At the usual slow growth rates of 1 μm/hr, the use of mechanical shutters allows for precise layer control and extremely abrupt interfaces.

The epitaxial growth of III-V semiconductors is accomplished by the following surface processes [Zangwill 1988]:

i) physisorption, which is the adsorption of the constituent atoms or molecules impinging on the substrate surface,

ii) surface migration and dissociation of the adsorbed molecules,

iii) chemisorption, or incorporation of the constituent atoms into the crystal lattice of the substrate or the epilayer already grown,

iv) thermal desorption of the species not incorporated into the crystal lattice.

A good deal of the kinetics of GaAs growth was learned from pulsed As_2 beam scattering studies [Foxon *et al* 1977]. The experiments measured the intensity of As_2 molecules scattered from a GaAs substrate with and without pre-dosing by a Ga beam. The results showed that atomic Ga and As_2 molecules adsorb onto GaAs surfaces rather differently; the sticking coefficient of Ga is unity (all of the incident Ga atoms stick on the substrate), while

the sticking coefficient for arsenic changes from one to zero as the coverage of gallium decreases, due to the formation of GaAs and an As-terminated surface. A growth model based on these experiments suggests that arsenic dimers initially adsorb into mobile precursor states. The As_2 dissociates so that bonding occurs as individual As atoms, but only above paired free gallium sites. The excess As_2 either desorbs, or associates with other dimers to desorb as As_4 molecules. Consequently, stoichiometric gallium arsenide still forms even when the flux of arsenic exceeds that of gallium. This type of mechanism is not unique to GaAs, but applicable to other III-V binary compounds [Farrow 1974]. For III-III-V ternary compounds, such as InGaAs, the sticking coefficients for both group III elements are unity, hence alloy composition is controlled by the relative fluxes of the group III elements in the beam in the presence of excess As_2.

It is important to note here that the III-V compounds, for example InP, are temperature unstable above the congruent evaporation temperature and this has certain consequences when depositing by MBE. At temperatures above congruent sublimation (~365 °C for InP) the group V element is preferentially desorbed, and an excess of the group V species is required to suppress liquid indium formation. At even higher temperatures (~575 °C for InP) the evaporation of the group III element becomes significant and the deposited layer thickness is less than anticipated from the group III arrival flux due to reevaporation. To maintain constant growth rates at these high temperatures a larger group III/group V flux ratio is needed. Consequently, when dealing with ternaries, the reevaporation of the more volatile group III component could alter the alloy composition.

The above considerations are thermodynamic in nature, and take into account key parameters such as the group V flux, substrate temperature and the group V/group III flux ratio. Some additional parameters not mentioned previously include substrate orientation and surface conditions such as impurities and defects. While these parameters alter the

thermodynamics, they also alter the kinetics of growth. In this work, the growth conditions of substrate temperature and the group V flux were varied in an effort to increase the growth rate, in specific regions, by altering kinetic processes such as adatom migration.

2.4 GROWTH STRUCTURE

A cross-sectional schematic of the grown heterostructure, used primarily for photoluminescence studies, is illustrated in figure 2.3. The structure consisted of a 1000 Å InGaAs reference layer and a 50 Å quantum well layer, nominally lattice-matched to InP, sandwiched between InP barrier layers. The thick InGaAs layer was used to measure the composition and to provide a reference for determining the quantum-size effect in the quantum well. The quantum well was grown near the top surface so that luminescence could be seen from both layers simultaneously. All the structures were grown undoped. Compositional nonuniformity arising from source alignment was minimized by sample rotation.

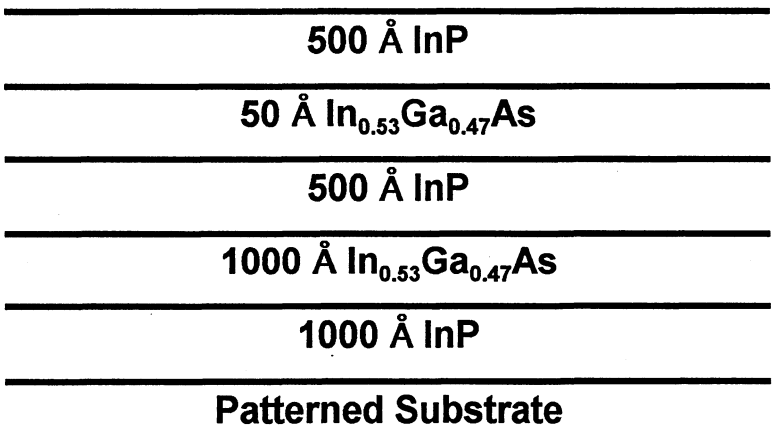

Figure 2.3: *Diagram of the MBE growth performed over the patterned substrate. All layers were grown undoped.*

2.5 GROWTH CONDITIONS

The objective of varying the growth conditions was to investigate the effect of the substrate temperature and arsenic flux on the magnitude of the bandgap shifts between waveguide stripes. The substrate was radiatively heated by a resistive element and the temperature controlled by a thermocouple positioned behind the substrate. An infrared pyrometer was used to estimate the surface temperature at the centre of the wafer. The substrate temperature was varied from 460 - 515 °C as measured by the pyrometer. For a growth rate of 1 μm/hr the total group III calculated flux is 5.5×10^{14} atoms/cm^2-sec. From previous calibrations an arsine flow rate of 1.9 sccm corresponds approximately to 2.8×10^{14} As_2/cm^2-sec (for a V/III ratio of one) or a minimum for stoichiometric growth. The arsenic dimer flux was varied by controlling the arsine flow rate from 2.2 to 6.1 sccm, which give corresponding V/III ratios of approximately 1.2 to 3.4.

TABLE 2.1: Growth Conditions

MBE Growth #	Temperature (C)	As Flow Rate (sccm)	V/III Ratio
1043	460	2.2	1.2
1044	460	6.1	3.4
1045	515	3.9	2.2
1162,1163, 1437	510	2.9	1.5

2.6 WAFER MOUNTING

The 15 mm x 15 mm InP substrates were attached to a molybdenum substrate holder with tungsten clips ready for insertion into the growth chamber. When it was necessary to

grow on smaller pieces, they were indium bonded on to a full size square piece and mounted. For some pieces, where the sample surface was predominantly covered with SiO_2, to obtain an unpatterned region for growth, the square substrates were indium bonded onto a quarter wafer.

2.7 GROWTH PROCEDURE

The procedures for growth were the same as for all standard planar growths performed at the Centre for Electrophotonic Materials and Devices (CEMD). Prior to growth, the sample was degassed for 15 minutes at 300 °C in a chamber vacuum-linked to the MBE growth chamber. Thereafter, the samples were transferred to the growth chamber. Since temperatures above the congruent evaporation temperature were needed for growth, once the temperature was in excess of 350 °C the sample was exposed to a phosphorous overpressure to prevent substrate decomposition. At a substrate temperature of 460 °C, the substrate was exposed for 2 minutes to an electron cyclotron resonance (ECR) hydrogen plasma to remove the protective InP native oxide formed by ultra-violet ozone cleaning. The growth consisted of an InP buffer layer deposited at a temperature of 460 °C at a growth rate of 1 μm/hour. The InGaAs was grown at 1 μm/hour previously calibrated at an InGaAs growth temperature of 500 °C and an arsenic flow rate of 3.9 sccm. A growth interruption of 2 minutes existed between the InP and InGaAs in order to ramp up the temperature and change the group V gas from phosphine to arsine. On some occasions a reflection high energy electron diffraction (RHEED) pattern was generated. A streaked diffraction pattern developed from the epitaxial growth while a ring diffraction pattern resulted from the polycrystalline layer deposited on the SiO_2 film.

2.8 DISCUSSION

Figure 2.4 is a Nomarski interference contrast micrograph illustrating the morphology of the surface after growth. Deposition occurred uniformly over the entire surface; however, epitaxial growth took place only in the selected areas, and the remainder was covered with polycrystalline material. As a result, the growth in the stripe area was flat and featureless,

Figure 2.4: *Nomarski micrograph of top view of the wafer after growth.*

while that on the SiO_2 developed a grainy texture. Figure 2.5 is a SEM photograph of an enlarged, cleaved cross-section of the layers including the window area and polycrystalline growth. A transition region (typically called edge growth) of approximately 1 μm in width, developed between the epitaxial and polycrystalline materials. Thus, useful mask dimensions are limited to greater than 2 μm.

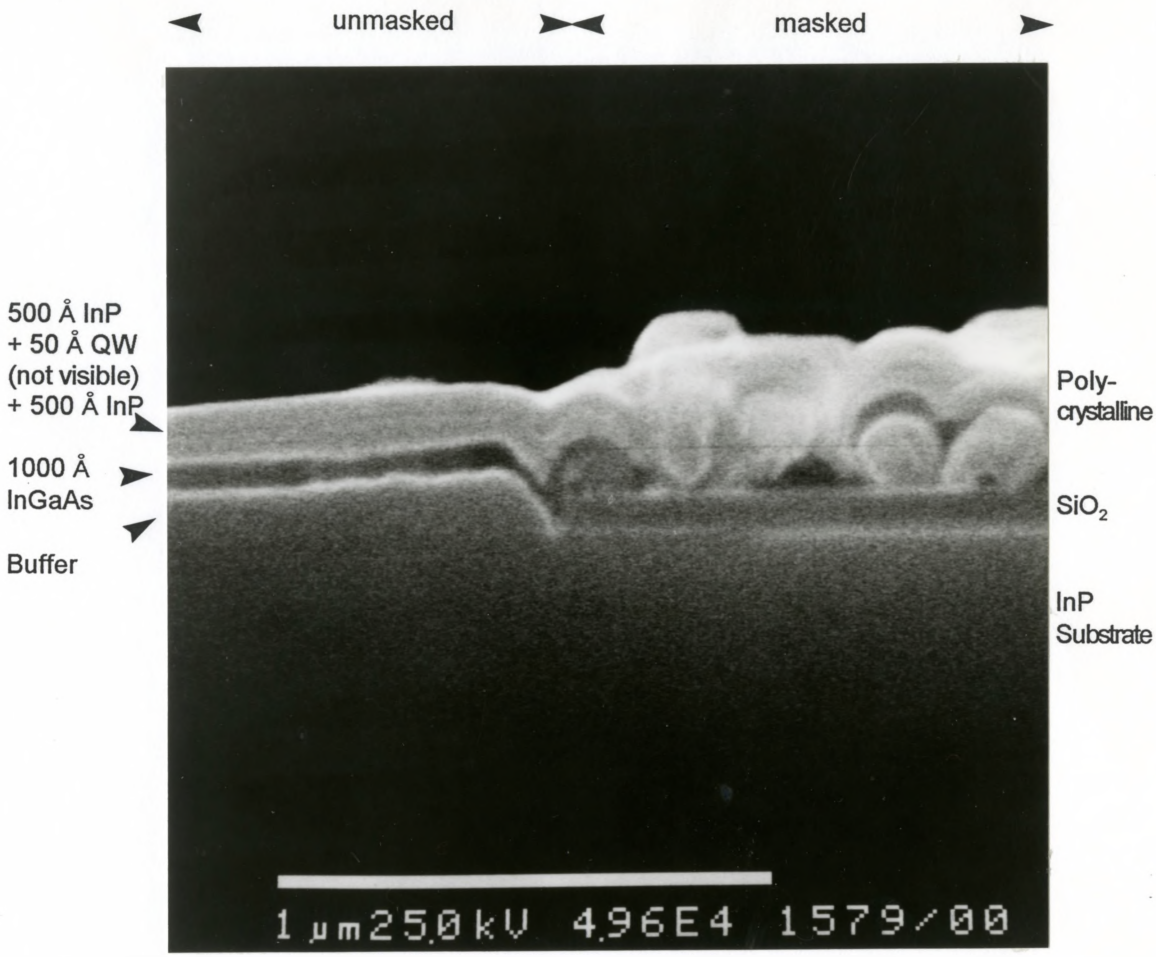

Figure 2.5: *SEM image of a cleaved cross-section of a multilayer device grown by GSMBE on (100) InP substrate and SiO_2. The device consists of 1000 Å InGaAs, 500 Å InP, 50 Å InGaAs and 500 Å InP. The InGaAs layers were grown nominally lattice-matched on an unmasked substrate. An etch was used to highlight the InGaAs layers.*

To prepare samples for SEM, a conventional stain treatment, consisting of immersion for about 2 seconds in $K_3[Fe(CN)_6]$:KOH:H_2O, was used to delineate the epitaxial layers. The sections were then mounted on end using conductive silver paint. Since undoped semiconductors are relatively poor conductors that exhibit charging artifacts under normal operating conditions, a conductive gold film coating (~8 nm) was sputtered on to the samples to significantly increase the resolution.

CHAPTER 3

STRUCTURAL AND SPECTRAL CHARACTERIZATION

3.1 INTRODUCTION

In this chapter, evidence of in-plane bandgap variations of the InGaAs epilayer growths, described in Chapter 2, is presented. Bandgap uniformity and crystal quality, within the centre of the stripe, appear to be good. Section 3.2 describes the most important experimental techniques: spectral photoluminescence (PL), scanning photoluminescence (SPL) and transmission electron microscopy (TEM). Section 3.3 provides analysis of the growths, and concentrates on: 1) bulk compositional determination and bandgap shift (3.3.1); 2) the quantum well shifts of the bandgap, for different mask dimensions and growth conditions (3.3.2); 3) uniformity of the bandgap across a stripe (3.3.3); 4) the quality of the epitaxial growth in the stripe (3.3.4); 5) edge effects (3.3.5); and finally a discussion of additional factors important for device applications (3.3.6).

3.2 CHARACTERIZATION TECHNIQUES

3.2.1 Photoluminescence

Photoluminescence (PL) is a sensitive, nondestructive technique which is used to analyze the spontaneous emission of semiconductors. Laser light, with an energy substantially greater than the bandgap energy of the semiconductor, is used to excite

electrons from the valence band to the conduction band. The carriers subsequently relax to their lowest available energy states near the band-edge and then recombine. In the case of radiative recombination, the resulting emission spectrum can be analyzed to determine properties of the material. At room temperature, band-to-band PL represents the dominant process, with the emission spectrum having a maximum at $h\nu=E_g+kT/2$ with a FWHM of 1.8kT. To view extrinsic transitions involving localized impurity states in the bandgap, low-temperature measurements are performed to minimize thermal broadening and therefore allow separation of similar energy transitions.

3.2.2 Photoluminescence of Quantum Wells

A single quantum well for electrons and holes is formed by a heterostructure in which a thin < 300 Å narrow bandgap material (ie. InGaAs) of thickness L_z is sandwiched between layers of wider bandgap material (ie. InP). An electron or hole travelling in the growth direction will become trapped in the quantum well and its energy will become quantized. The photon energy of the n=1 heavy hole recombination is $h\nu=E_g+E_e+E_h$ where E_g is the three-dimensional bandgap energy, E_e and E_h are the energy shifts of the n=1 electron and heavy hole levels as calculated from the time-independent Schrödinger equation. The measured energy shift, compared to the bandgap energy of the well material, is referred to as the quantum-size effect and depends on the width of the well.

3.2.3 Spectral Photoluminescence System

The McMaster University PL system is illustrated in figure 3.1. The excitation source is a 20 mW, 488 nm argon laser focused to a ~0.1 mm spot on the sample surface. A spectrometer, with a 600 lines/mm grating (for the wavelength range of 800 - 1800 nm) was used with an InGaAs detector to measure the emitted light. The entrance and exit slits of

the spectrometer were 500 μm which corresponds to a wavelength resolution of 1 nm, or 0.6 meV. All of the spectra were corrected for the spectral response of the detector system. Preparation for low-temperature photoluminescence measurements, at 11K, involved cleaving small sections of samples, mounting them onto a copper block with silver paste, and placing them into a closed-cycle helium cryostat.

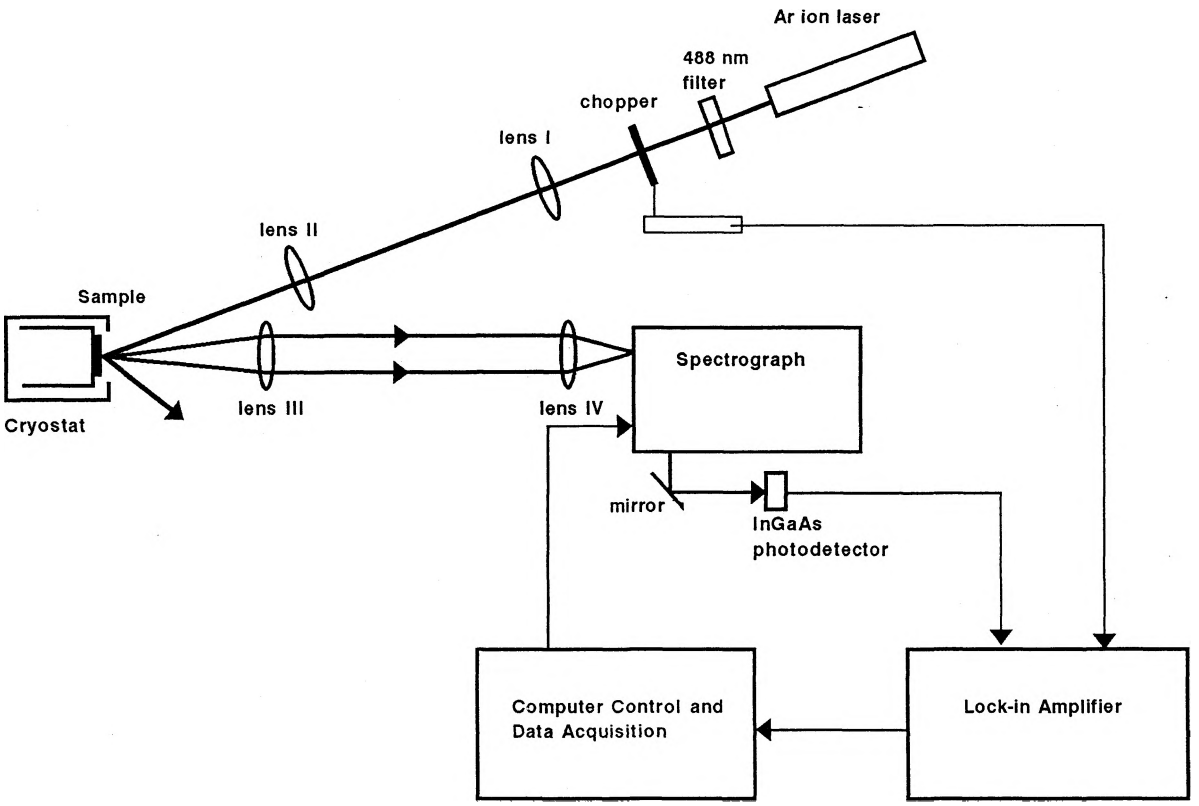

Figure 3.1: *Photoluminescence imaging system at McMaster University.*

3.2.4 Scanning Photoluminescence System

Spatially resolved scanning photoluminescence measurements were carried out at room-temperature using the SCAT-SPEC IMAGEUR of SCANTEK (France), as illustrated in figure 3.2. The photoluminescence signal was excited with a He-Ne (632.8 nm) laser

which was focussed to a 1 μm spot size. A spectrometer (Oriel 77200), with a 300 lines/mm grating (for the wavelength range of 1330 - 3000 nm) was used with a liquid-nitrogen cooled InAs photodetector to measure the emitted light. The wavelength resolution was 1 nm.

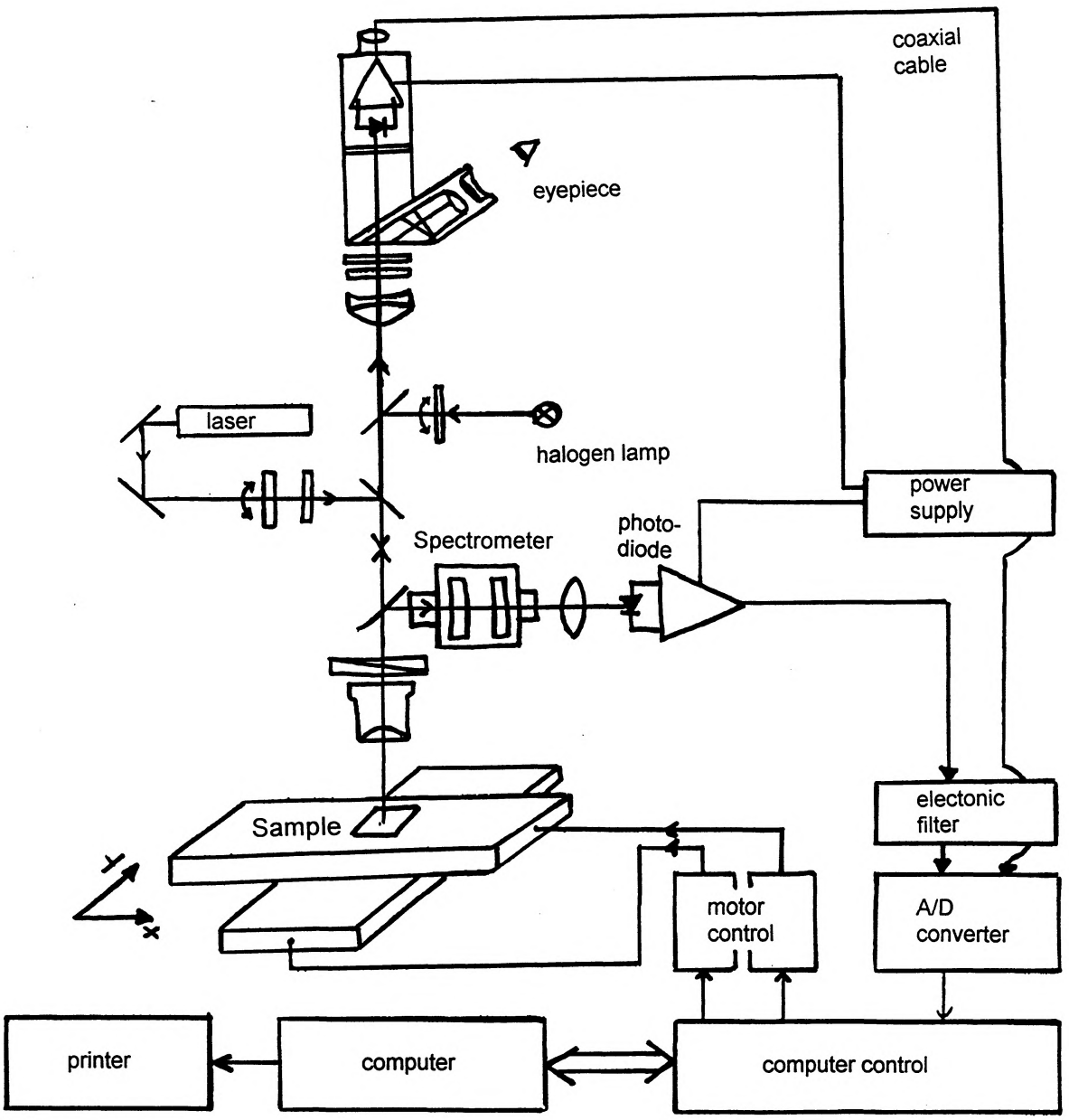

Figure 3.2: *Scanning photoluminescence imaging apparatus at Ecole Centrale Lyon.*

3.2.5 Transmission Electron Microscopy

Transmission electron microscopy is a technique based on the passing of electrons through a very thin sample. The primary electrons which enter the top of the sample are either transmitted through the sample, or diffracted if the particular atomic planes encountered satisfy the Bragg condition relative to the angle of the incident beam. Depending on the operating mode of the TEM, either a magnified image or a diffraction pattern from the specimen can be viewed on a fluorescent screen.

If the viewing screen is focused at the image plane, a bright-field image is produced by placing an objective aperture after the objective lens to allow only the transmitted beam to form the contrast image. Similarly, if the viewing screen is focused at the diffraction plane, a diffraction pattern consisting of a regular array of spots appears, which corresponds to the different planes aligned at the Bragg condition. If the specimen is polycrystalline, the diffraction pattern is the superposition of the individual patterns of all orientations satisfying the Bragg condition, and the spots tend to form on to concentric rings [Goodhew *et al* p. 45 1988]. If the specimen contains very many crystals of random orientations the spots on the rings are so close that the rings appear continuous. Therefore, TEM analysis not only reveals the morphology but also the atomic structure of a region.

In this work, a 120 kV electron beam was used to produce bright-field images of various cross-sectional TEM samples which were prepared from stripes along the [011] direction. To prepare the samples, the wafers are cut into millimetre-thick slices and glued together on edge in a holder for polishing, disc cutting and dimpling down to 50 μm. Electron transparent thicknesses of 500-1000 Å were achieved by ion milling. Care must be taken when ion milling because different materials erode at different rates. Even though preparation is labour intensive, cross-sectional TEM samples have the advantage of providing direct examination of the planarity and defects associated with a thin-film interfacial

microstructure.

3.3 RESULTS

3.3.1 Compositional Determination of the Bulk

Room-temperature spectral PL measurements were performed on areas of constant stripe width. A set of typical sample spectra, showing both the bulk and quantum well peaks are illustrated in figure 3.3. The equation presented by Kuphal was used to determine the composition of the bulk alloy layer from the peak PL energy spectrum [Kuphal 1984], which was corrected for strain due to the lattice mismatch between the epilayer and the substrate [Asai *et al* 1983]. The equations used have been included in the appendix. The strain

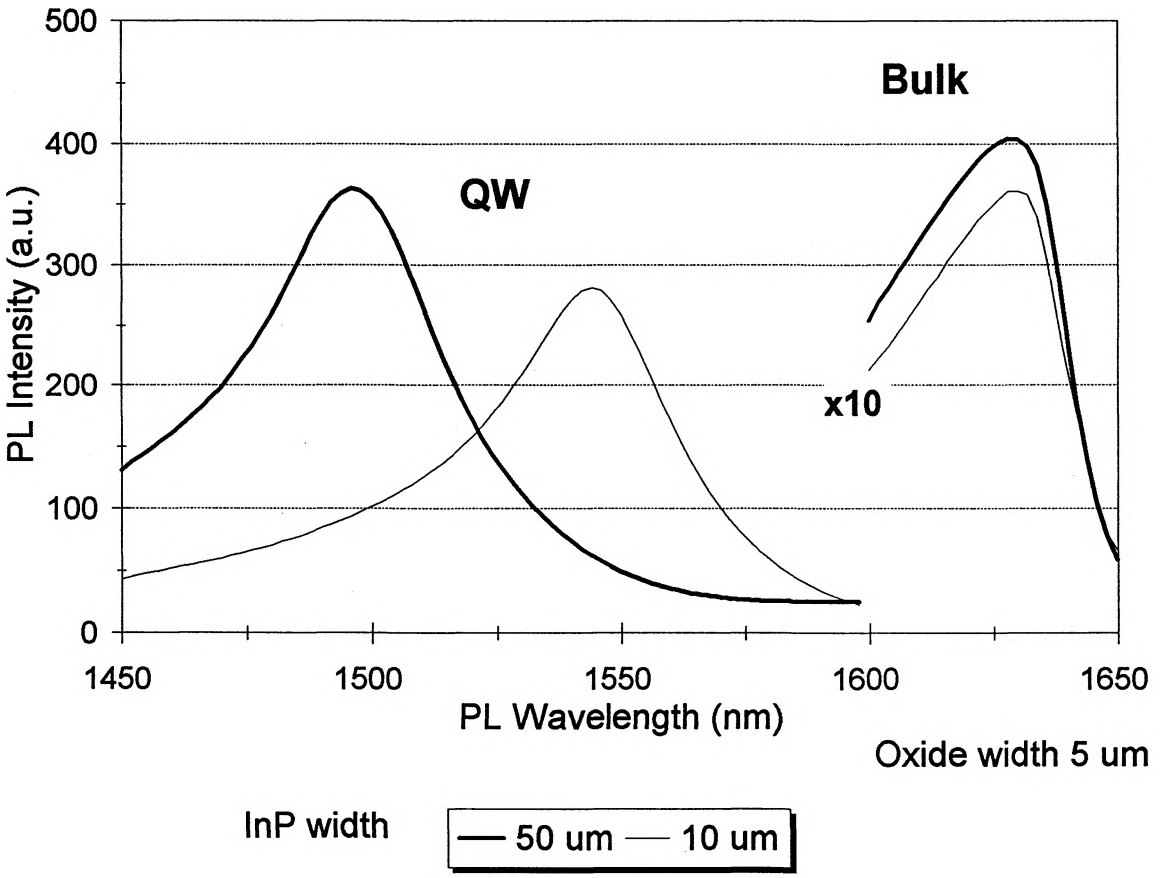

Figure 3.3: *Room-temperature photoluminescence spectra from sample #1437, showing the bulk peak and the quantum well peak for widths of (50,5) and (10,5).*

induces modifications of the energy-band structure which must be taken into consideration when calculating the composition. The samples were grown nominally lattice-matched, with peak PL wavelengths in the range of 0.75 ± 0.01 eV. Background measurements were performed either on an unmasked region, or with a very large stripe width (50 μm) and small SiO_2 width (10 μm). All samples were grown within a 1% change in the InGaAs alloy composition compared with lattice-matched conditions, which corresponds to a calculated 10 meV change in the bandgap. Similar measurements were preformed for narrower slit widths to examine the change in composition; however, no wavelength shift was observed when compared with background readings, even at low temperatures.

3.3.2 Quantum Well Peak Wavelength Shift

In this section, the shift of the InGaAs quantum well photoluminescence peak wavelength for various growth conditions and mask dimensions will be discussed. All quantum well shifts were referenced to the largest stripe width to minimize any slight compositional or thickness changes due to simple sample-to-sample variation. The peak wavelength of the largest stripe width (50 μm), and background readings, were located at approximately 1500 nm. When it was possible to measure the background QW peaks at various positions on the sample (MBE#1437), good uniformity was demonstrated arising from sample rotation. The peaks shifted by a maximum of 5 nm (~2 meV), significantly smaller than shifts experienced by masking.

3.3.2.1 Growth Conditions

Figure 3.4 illustrates the peak wavelength of the InGaAs quantum well for various arsine flow rates and substrate temperatures. The InP waveguide stripes ranged from 5 μm to 50 μm wide with a constant SiO_2 width of 10 μm. As the InP width decreases, the peak wavelength is increasingly red-shifted. The largest shift, of 55 nm, occurred for the narrowest stripe and for growth conditions of low arsine flow rate and high substrate temperature.

These conditions are consistent with the discussion in section 2.3 detailing how varying the growth parameters influences the kinetics of surface migration. By decreasing the flow rate and increasing the temperature the adatom diffusion length is increased.

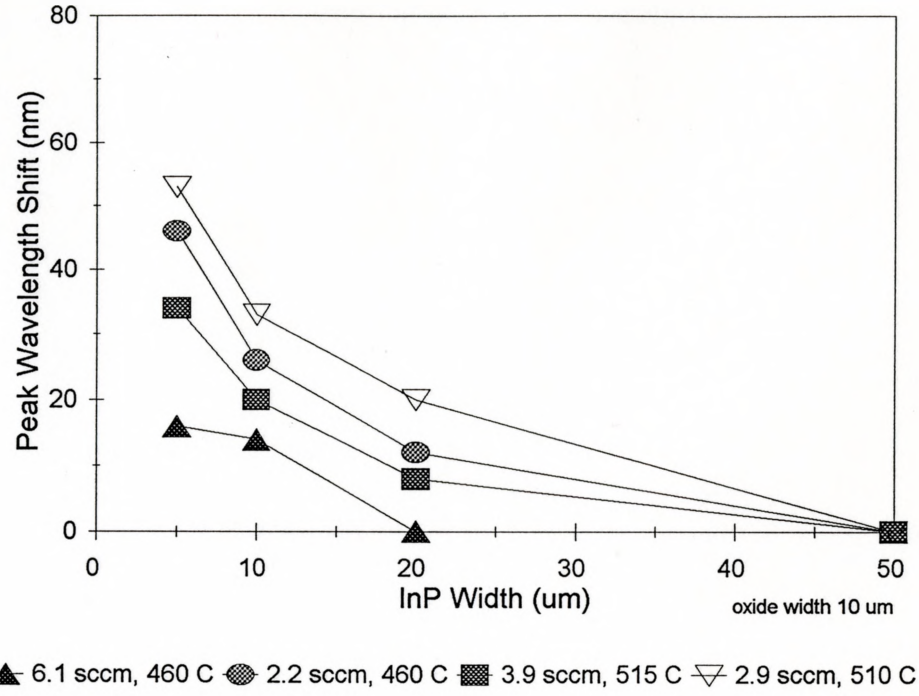

Figure 3.4: *The peak wavelength shift of the room-temperature PL e1-hh1 transitions with growth conditions for the InGaAs quantum well.*

3.3.2.2 Stripe Dimensions

From the conditions of maximum wavelength shift (AsH_3 = 2.9 sccm and substrate temperature = 510 °C) additional growths were performed, but this time varying the oxide width. Figure 3.5 illustrates the peak PL wavelength shift (MBE#1163) for different InP widths and oxide widths. For a given InP width, for example 20 μm, as the oxide width increased from 1 μm to 5 μm a larger red-shift occurred. A dependence on mask width suggests that this effect can be explained in terms of migration from the region of the mask material to the stripe openings, ie. larger mask widths provide a greater group III source. The increased red-shift occurs for oxide widths up to 5 μm, with no significant red-shift

beyond that.

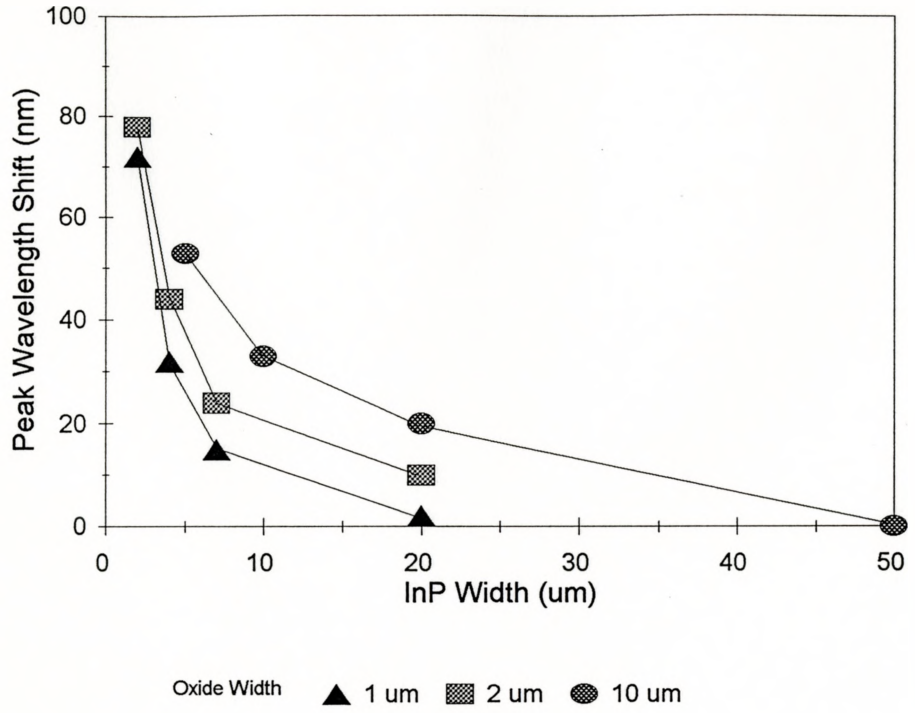

Figure 3.5: *The peak wavelength shift of the room-temperature PL e1-hh1 transitions with mask dimensions for the InGaAs quantum well.*

3.3.2.3 FWHM and PL Intensity

Figure 3.6 illustrates the linewidths for the PL scans presented in figure 3.4. While there is slight sample-to-sample variation, within a given sample there is no significant dependence of broadening on stripe width. The values of the FWHM are on the order of kT, consistent with thermal broadening.

Figure 3.7 illustrates the decrease in the integrated PL intensity as the waveguide stripes get narrower. The laser beam diameter is large, covering both monocrystalline and polycrystalline material, so the intensity values have been corrected for the effective stripe area. Non-radiative recombination at the growth edges could be causing the decrease in PL intensity, which is more dramatic at narrow stripe widths. Since the PL intensity is an

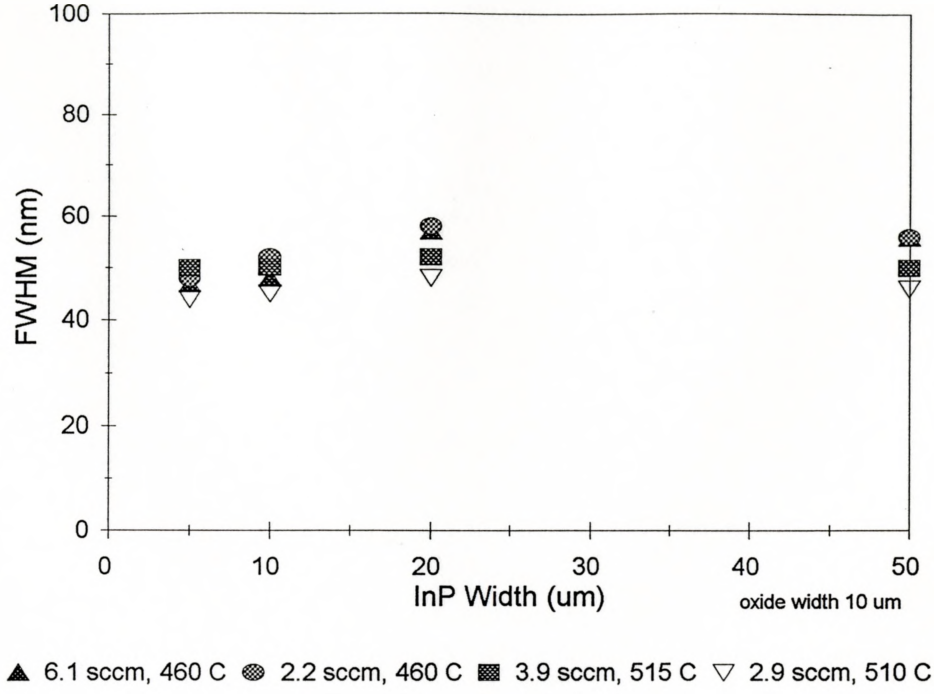

Figure 3.6: *The distribution of linewidths of the room-temperature PL e1-hh1 transitions for the InGaAs quantum well.*

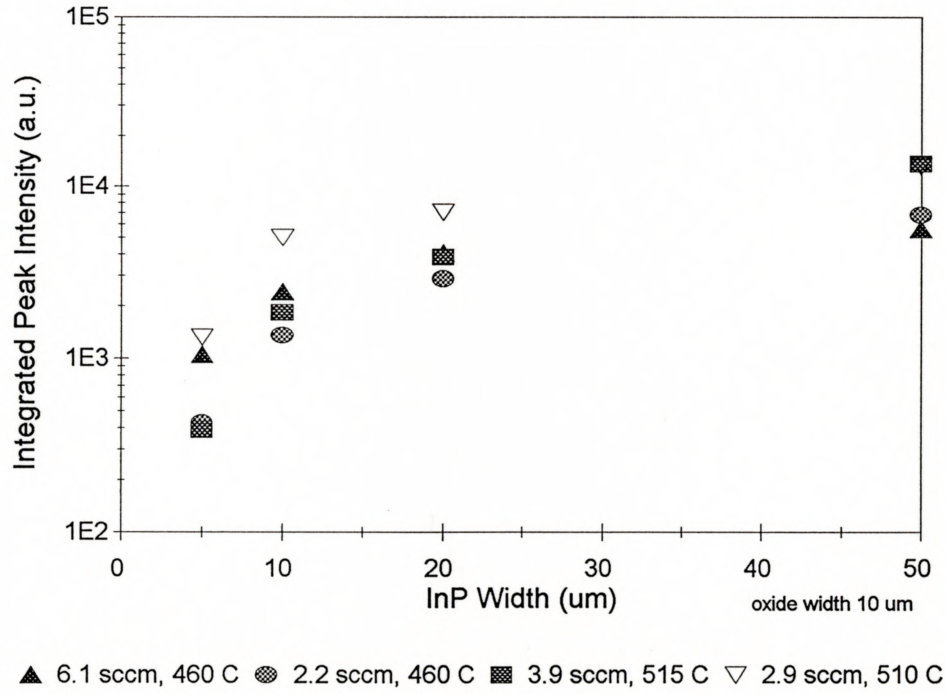

Figure 3.7: *The distribution of room-temperature integrated PL peak intensity for the InGaAs quantum well.*

indication of the crystal quality, scanning PL was used to examine the change of the epilayer quality and also bandgap across the stripe.

3.3.3 Variation of Peak Wavelength across the Stripe

Figures 3.8 to 3.10 illustrate the peak wavelength at positions across the sample for the three different growth conditions, with InP widths of 5 μm and 10 μm. An average value of the central region is indicated to the right of the graphs. For the condition of high arsenic overpressure (#1044) no difference was noted between the central positions of the different width stripes; while for the high substrate temperature (#1045) and low arsenic overpressure (#1043) conditions, the 5 μm stripe was red-shifted by 25 nm. Within the central region, the peak wavelength varied by ± 3 nm. It can be observed from the scans that the edges are additionally red shifted by about 10 nm due to the diffusion profile. A similar profile was examined by Bulitka [1993] who calculated the diffusion length of indium to be 2.5 - 3.5 μm. Since those layers were very thick, quantum size effects were negligible and the shift was due to diffusion of indium adatoms out of V-grooves with (111)B sidewall facets.

Figure 3.11 illustrates a 4K cathodoluminescence (CL) scan of a (7,2) stripe from MBE#1163, which was generated at Oxford Instruments in England. This graph illustrates the distribution of the bulk InGaAs peak at the wavelength of 1586 nm. For CL an electron beam was used to excite the sample and the intensity of a specific photon wavelength plotted, red indicating a high intensity. This technique can be used to perform peak distribution mapping. The figure shows the uniformity of the sample stripe and easily illustrates non-uniformities due to masking. At this wavelength the photons emitted are from the bulk epilayer, so any variations in thickness do not contribute to a change in photon wavelength, only compositional variations. To precisely determine how the composition changes, more scans at other wavelengths would be needed to be compared.

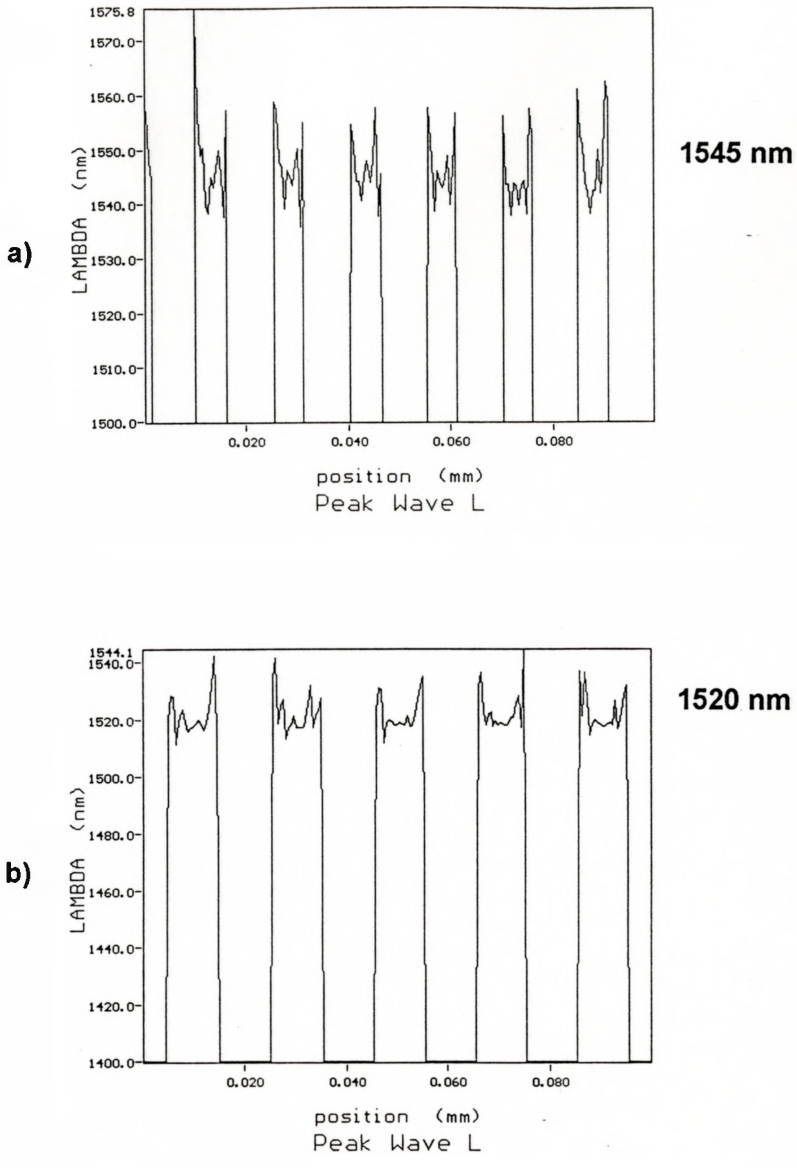

Figure 3.8: *SPL of the quantum well peak wavelength with position on the sample. The values beside each graph indicate the average peak wavelength of the centre of the stripe. The sample was #1043 a)(5,10) and b) (10,10).*

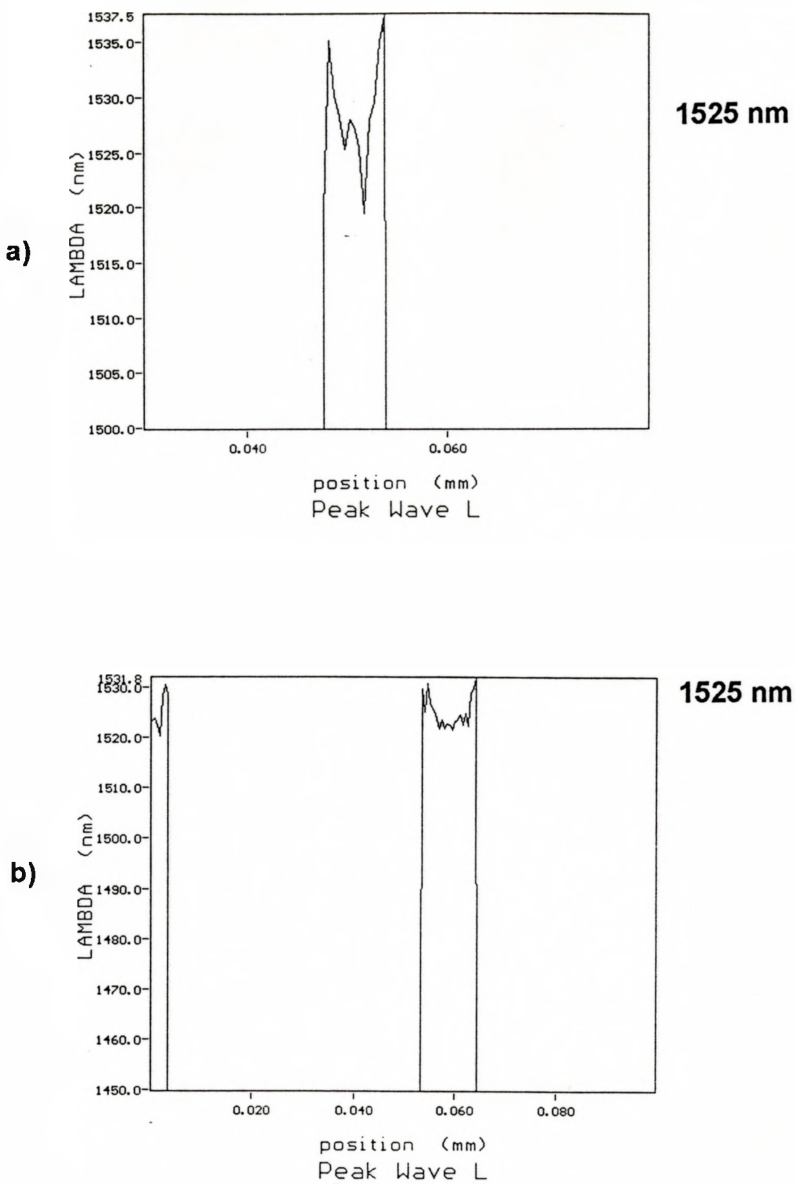

Figure 3.9: *SPL of the quantum well peak wavelength with position on the sample. The values beside each graph indicate the average peak wavelength of the centre of the stripe. The sample was #1044 a)(5,50) and b)(10,50).*

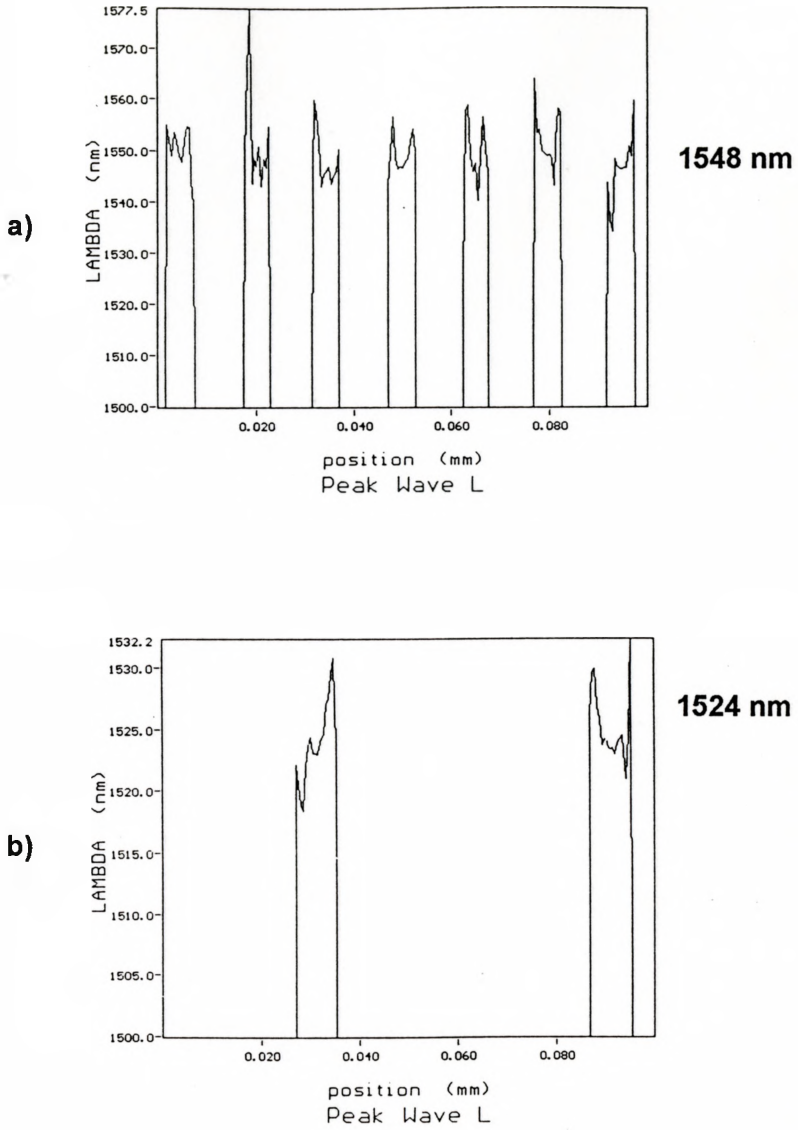

Figure 3.10: *SPL of the quantum well peak wavelength with position on the sample. The values beside each graph indicate the average peak wavelength of the centre of the stripe. The sample was #1045 a)(5,10) and b)(10,50).*

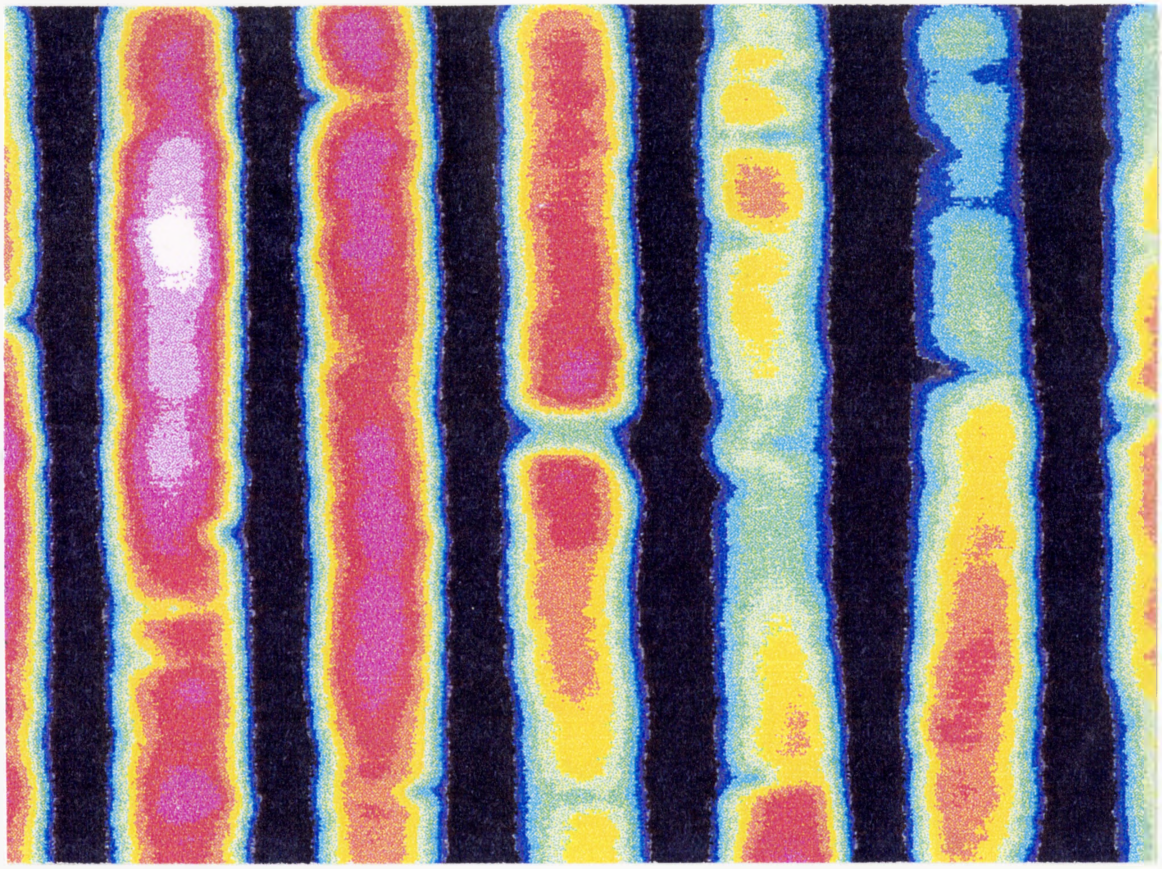

Figure 3.11: *Cathodoluminescence image taken at 4K for a slit width of (7,2). The image represents the intensity of photons emitted at the bulk peak wavelength of 1586 nm. The black stripes represent areas of no photon emission corresponding to the polycrystalline material deposited on the SiO_2.*

3.3.4 Variation of Epilayer Quality across the Stripe

Figure 3.12 illustrates the peak intensity across a patterned sample. The maximum PL intensity occurs at the centre of the InP stripe, which corresponds to better quality material. A TEM cross-sectional [011] axial bright-field image is illustrated in figure 3.13 for sample MBE#1437 and slit width of (50,10). From TEM, the central region of the sample is high quality, free of dislocations and interfacial defects, which accounts for the good photoluminescence efficiency. Even for small slit widths, down to 5 μm, no interfacial defects were evident in the central region; however, from scanning PL a slight decrease of

a)

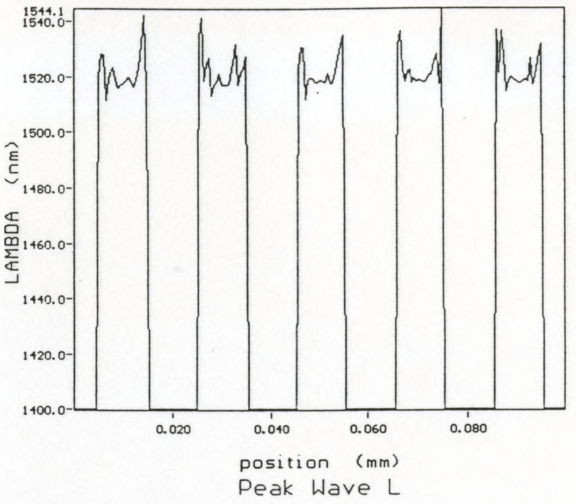

b)

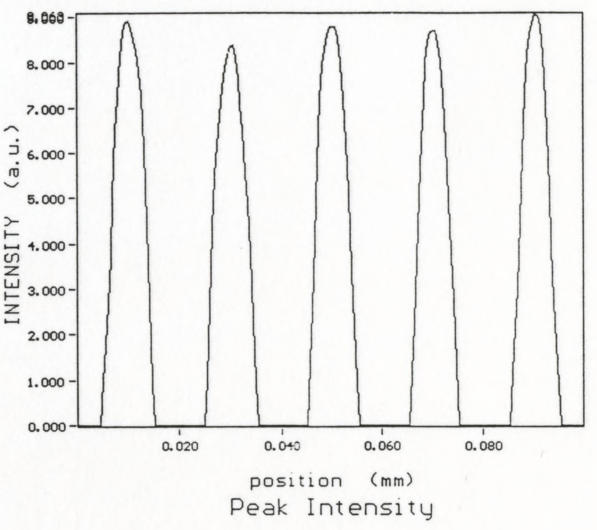

Figure 3.12: *a) SPL of the quantum well peak wavelength with position on the sample; b) plot of the intensity of the peaks in a). Notice that there is no photoluminescence coming from the material deposited on the oxide.*

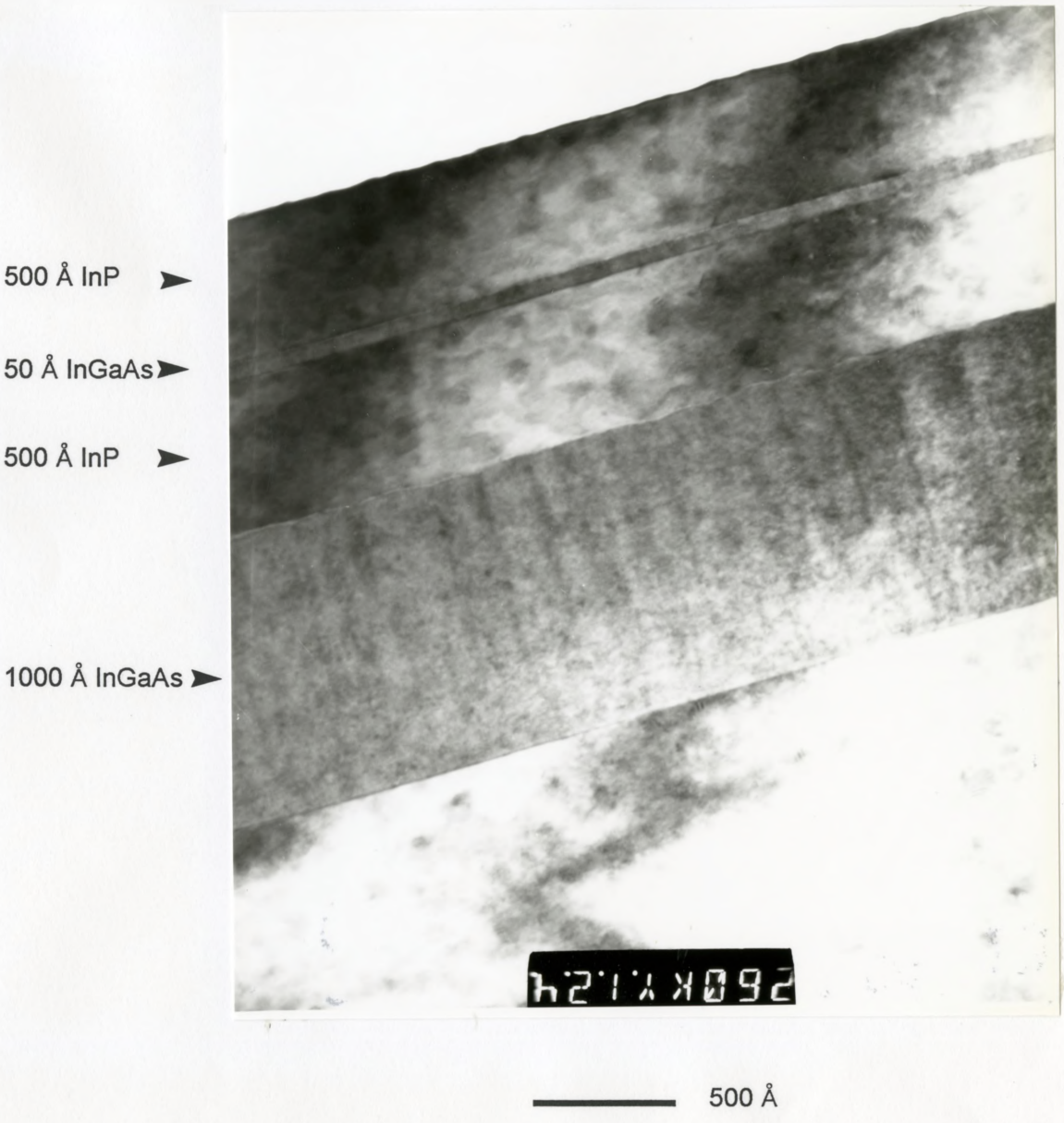

Figure 3.13: *A bright-field [011] axial TEM cross-sectional image of the centre of an epitaxial stripe width 50 µm, which was used for measurements of thickness. The interfaces are free of defects. The magnification of this image is 260,000x.*

the intensity occurred with decreasing stripe width.

Figure 3.14 illustrates a [011] axial bright-field TEM image of the edge growth. This transition region between monocrystalline and polycrystalline areas gives rise to {111} stacking faults [Goodhew *et al* p.83 1988]. Non-radiative recombination occurs at the defects which reduce the photoluminescence efficiency. No photoluminescence occurs for the material deposited on the oxide, which from diffraction TEM was determined to be polycrystalline.

3.3.5 RIE Removal of Edge Growth

Figures 3.15 and 3.16 illustrate the spectral PL scans associated with the quantum well taken at low temperatures. The samples before etching showed multiple peaks for both 10 μm and 50 μm slits. The observation of more than one emission band from a single quantum well implies that there are a few spatially distinct states, all with different energies. It has been shown that small inhomogeneous contributions such as compositional variations and graded interfaces tend to increase the linewidth or even split the peak into doublet or triplet peaks corresponding to different islands of growth [Herman *et al* 1991]. These additional peaks could therefore be due to variations of the well width and alloy composition between the centre and edge, or simply defects associated with the edges.

To remove the edge growths, a 5 μm SiO_2 stripe was photolithographically defined in the centre of the epitaxial growth on 10μm and 50 μm slits. Since a CH_4 RIE plasma will not etch SiO_2, a 5 μm ridge remained after the edge growth and polycrystalline material had etched away. After etching the sample, PL measurements were again performed and only the higher energy peak remained. Compared with unetched samples, the FWHM of the room-temperature scan decreased and the integrated PL intensity increased slightly. Since the ridges were not passivated, surface recombination effects could explain the lower than

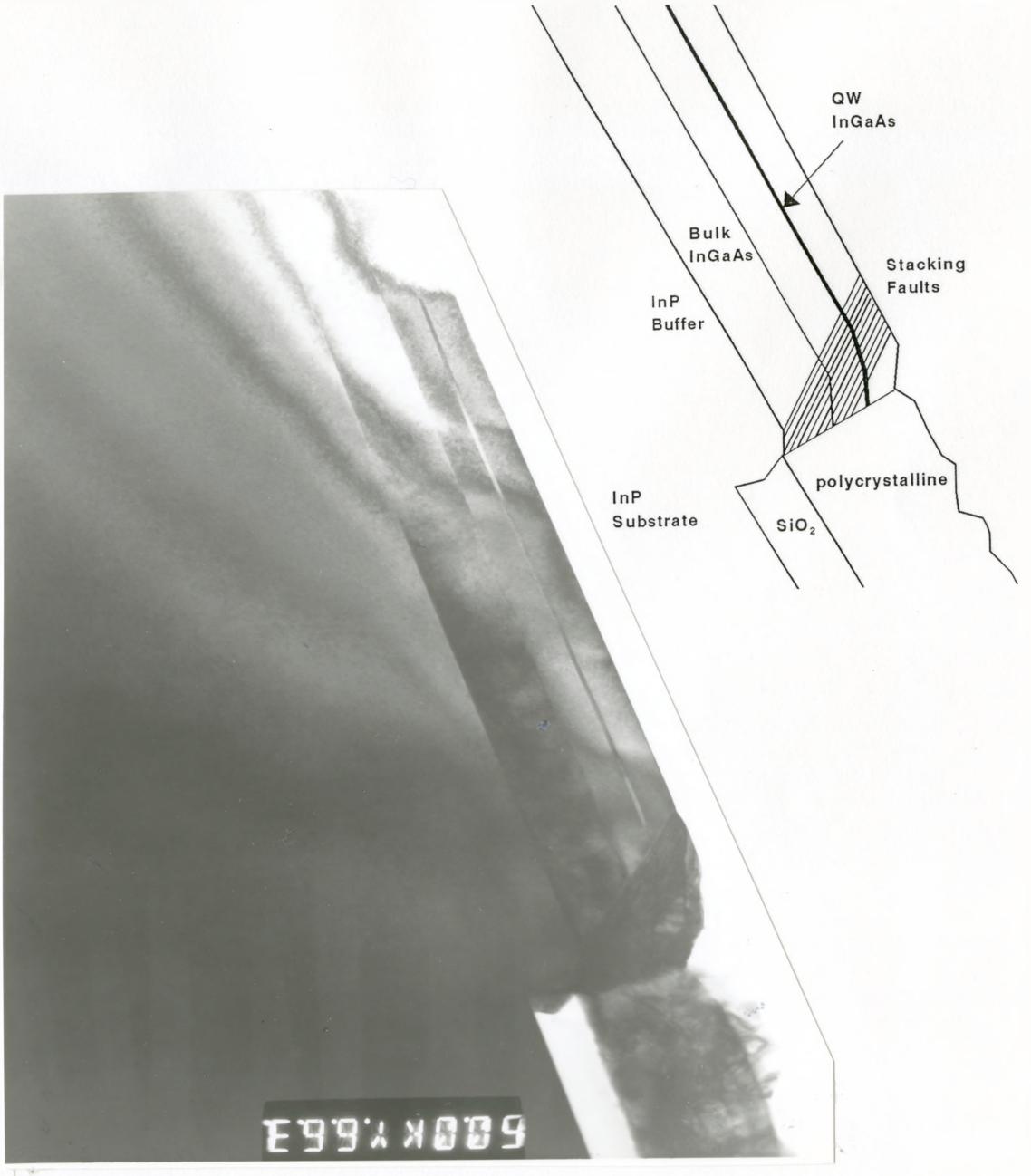

Figure 3.14: *A bright-field [011] axial TEM cross-sectional image of the edge growth. The magnification of this image is 60,000x. Notice the stacking faults at the edges.*

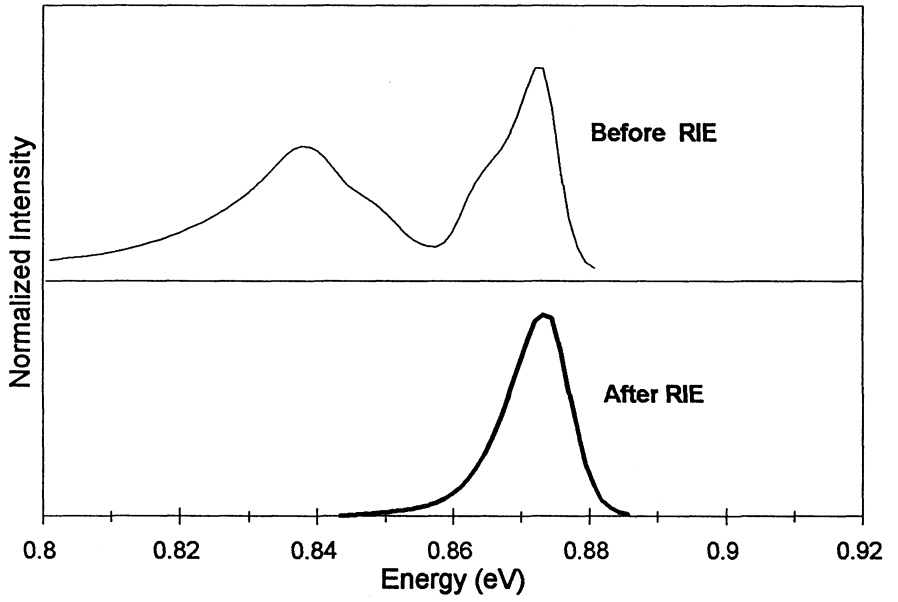

Figure 3.15: *11K photoluminescence spectra of the peak(s) corresponding to the quantum well before and after etching of the edge growth and the polycrystalline region. After etching only a 5 μm stripe was left in the centre of the epitaxial growth, which was originally 10 μm. The distance between ridges is 10 μm.*

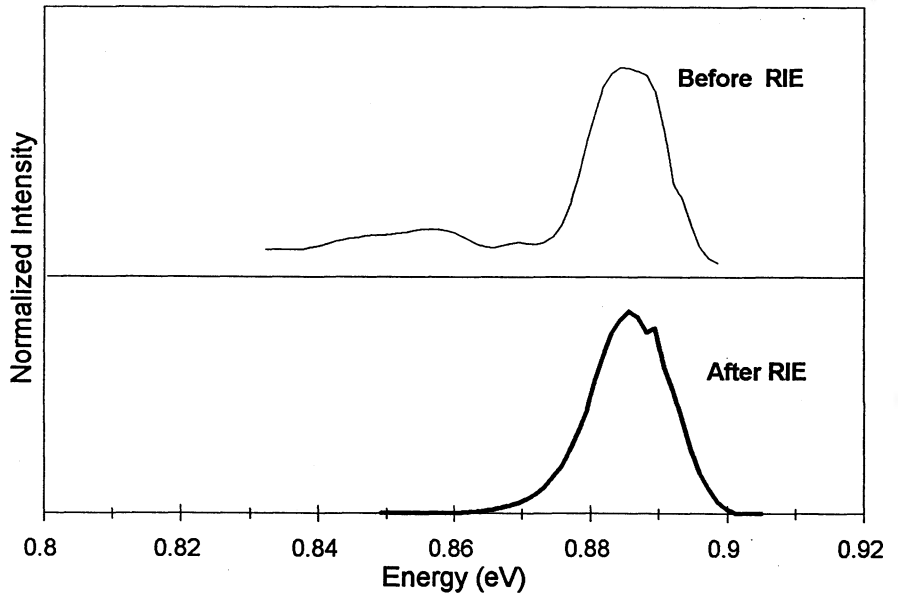

Figure 3.16: *11K photoluminescence spectra of the peak(s) corresponding to the quantum well before and after etching of the edge growth and the polycrystalline region. After etching only a 5 μm stripe was left in the centre of the epitaxial growth, which was originally 50 μm. The distance between ridges is 50 μm.*

expected PL intensity increase.

3.3.6 QW Thickness Measurements

From figure 3.13, measurements of the InGaAs quantum well for a (50,5) stripe indicate the thickness is closer to 61 ± 3 Å with the bulk layer at 986 ± 3 Å. For a very narrow stripe width of (5,10) the measured quantum well thickness was 72 ± 3 Å with the bulk layer at 1125 ± 3 Å, which represents an increase of 10 - 20%. This thickness increase for the quantum well translates into a shift of the PL spectra. At a thickness of 60 Å the bandgap energy of the quantum well is calculated by using the Schrödinger model with a conduction to valence band offset of $\Delta E_c = 0.39\ \Delta E_g$ [Forrest *et al* 1984]. For a change in peak wavelength of 50 nm, the quantum well would need to increase by 25 Å if only thickness variations were the case, instead thickness variations accounted for two-thirds of the increase. The additional shift could arise from an indium rich composition because the diffusion length of indium is greater than that of gallium [Arent *et al* 1989]. A change of 1% in the alloy composition would be needed for a match to experimental data; however, measurements from the bulk peak do not illustrate any shift.

3.3.7 Discussion

Figure 3.17 is an axial TEM image illustrating the small contrast oscillations evident in the reference layer. This is spinodal decomposition of InGaAs, where the modulations are indium-rich and gallium-rich regions [LaPierre 1994]. These In-rich and Ga-rich areas set up localized regions of strain, both compressive and tensile which cause the top of the bulk InGaAs layer to become bumpy as can be seen in figure 3.13. To increase the bandgap shifts, growths at high temperatures and low arsenic overpressures are needed; however, such conditions encourage spinodal decomposition. Whether this will seriously impact the function of a device is currently unknown.

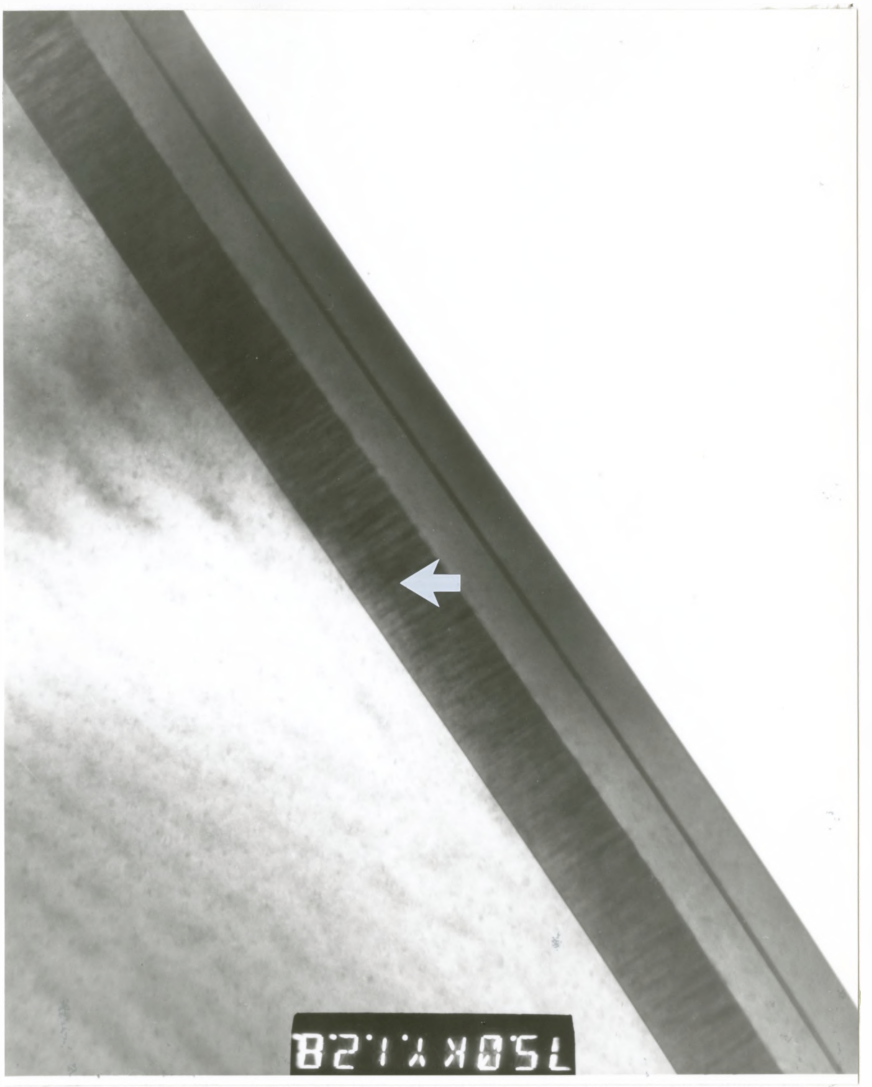

Figure 3.17: *A bright-field [011] axial TEM cross-sectional image of the centre of an epitaxial stripe width 50 μm. The thick dark layer is the bulk InGaAs with the quantum well InGaAs separated by 500 Å InP. The spinodal decomposition is evident in the bulk InGaAs layer. The magnification of this image is 75,000x.*

CHAPTER 4
LIGHT-EMITTING DIODE

4.1 INTRODUCTION

In the previous section significant bandgap shifts of 25 meV were illustrated using photoluminescence on undoped structures. Since selective-area deposition will eventually be used for device applications, this chapter describes a simple p-n junction light-emitting device pumped electrically (ie. electroluminescence) and the resulting shift in the spontaneous emission spectrum presented. Section 4.2 discusses the growth structure and fabrication process to produce a quantum well light-emitting diode (LED). Characterization of the diode including I-V and L-I curves, and the light output spectrum are illustrated in section 4.3. Finally, section 4.4 will provide some concluding remarks.

4.2 FABRICATION

The stripe-contact light-emitting diode which was fabricated is illustrated in figure 4.1. In this type of device, the current path is defined by using an oxide mask to limit the ohmic contact area. Before epitaxial growth the substrate was dielectric-patterned with InP stripe widths of 10 μm and 50 μm, with an SiO_2 width of 5 μm. The growths were performed and device processing carried out with the same procedure as used on planar substrates. The metal contact stripe was 5 μm in width and centred on the monocrystalline material. Carrier

confinement in the active region was provided laterally by the top current-blocking silica layer and also vertically by the heterostructure.

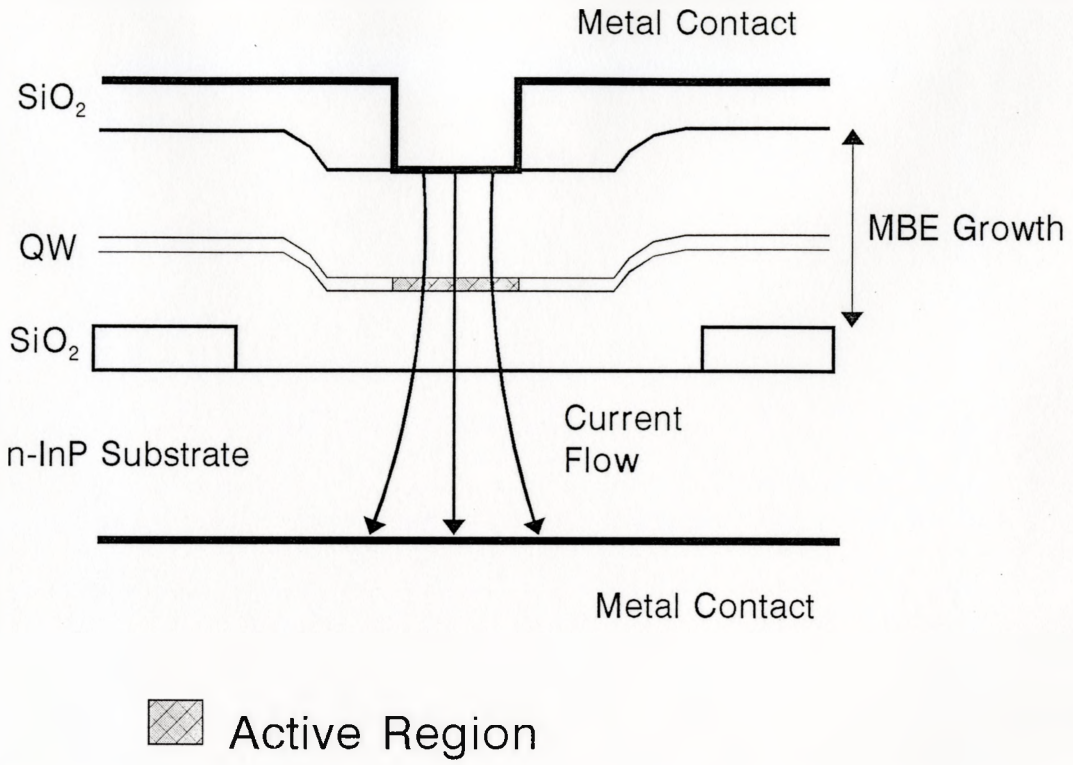

Figure 4.1: *Fabrication of stripe contact light-emitting diode. The stripe widths of the bottom patterned substrate is (50,5) and (10,5). The MBE growth is illustrated in Figure 4.2. The top metal contact is 5 μm.*

4.2.1 MBE Growth Structure

The double heterostructure LED is illustrated in figure 4.2. The active layer consisted of an intrinsic 50 Å nominally lattice-matched InGaAs quantum well, while the separate confinement region was defined by two intrinsic 750 Å InP layers. The difference between the InGaAs and InP layers (band offsets) provides carrier confinement used to help in recombination within the active region. The InP region has the purpose of confining the

optical power and also the injected carriers in the vicinity of the active region. Generally, this is an InGaAsP layer with an intermediate bandgap; however, since InGaAsP materials have not been tested, InP was chosen for this run. This undoped region was then sandwiched between n-type and p-type InP semiconductors which have a wider bandgap than the active region (and usually the confinement layers). A top p+ InGaAs contact layer is normally deposited to assure low series resistance [Temkin *et al* 1981], but for this LED the shift in emission spectrum measured at 1.5 μm was to be due solely to the quantum well.

1000 Å p^{++}-InP ($1x10^{19}$)	contact layer
1000 Å p-InP ($1x10^{18}$)	capping layer
750 Å InP (undoped)	confinement layer
50 Å $In_{0.53}Ga_{0.47}As$ (undoped)	active region
750 Å InP (undoped)	confinement layer
1000 Å n-InP ($1x10^{18}$)	buffer layer
n+ Patterned Substrate	

Figure 4.2: *Schematic of the growth structure (MBE#1255) used for the light-emitting diode. The undoped InP layers provide optical guiding and the recombination is performed in the quantum well layer. The InGaAs layer was grown at high substrate temperatures (510 °C) and low arsenic overpressure (AsH_3 = 2.9 sccm).*

4.2.2 LED Processing

After growth the current-blocking silica layer, consisting of 1000 Å of SiO_2, was deposited and a 5 μm stripe opened up down the centre of the epitaxial growth. The top p+ metal contact of Ti / Pt / Au (250 Å / 450 Å / 1500 Å) was deposited. The LEDs were then thinned and polished to approximately 150 μm, cleaned in organic solvents and the back n+ metal contact of Ni / Ge / Au (250 Å / 500 Å / 1500 Å) was deposited. The devices were annealed at 400 °C for 30 seconds and then cleaved (length of 500 μm) to form the Fabry-

Perot cavity. It was not possible to cleave individual dies, but blocks of approximately 10 devices were used for testing purposes.

4.3 CHARACTERIZATION TECHNIQUES

The LED devices were placed on a copper heat sink and a forward-bias current was applied across the device. All measurements were taken in continuous-wave mode and at room temperature. The light output was measured with a p-i-n detector placed against the device facet. Data acquisition was achieved by a computer program which allowed remote control of the equipment through a IEEE-488 bus. The computer program allowed data collection of light output versus current (L-I), voltage versus current (V-I) and by the addition of a spectrometer between the diode and the detector, the spontaneous emission spectrum.

4.3.1 L-I and I-V Curves

Figure 4.3 illustrates typical current-voltage (I-V) measurements of a processed light-emitting device. The reverse-biased leakage current is a direct indication of the lower quality epitaxial growth which may occur at the edges. Since the defect edges are closer to the active region for the 10 μm stripe than the 50 μm stripe, it would be expected to have the greater leakage current. It has been reported that after etching the edges, the leakage current was reduced by as much as 3 orders of magnitude [Hamm *et al* 1992] in an InGaAs/InP heterojunction bipolar transistor.

Figure 4.4 illustrates the light output with pump current (L-I), indeed the intensity of the light from the 50 μm stripe is greater than from the narrower stripe. From these graphs the external efficiency was calculated to be approximately 0.1%.

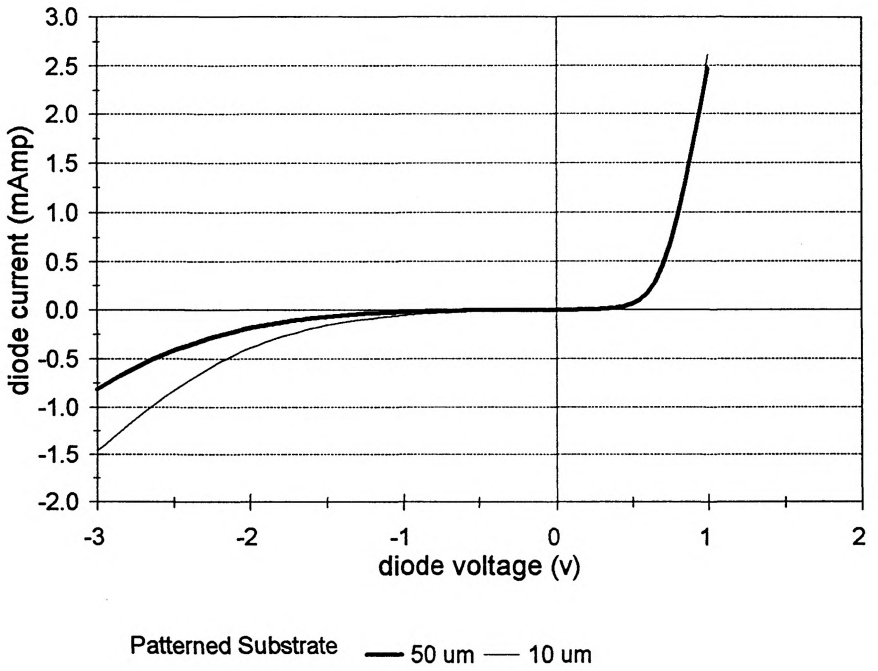

Figure 4.3: *I-V curve of the LED taken at room-temperature.* The cavity length is 500 μm.

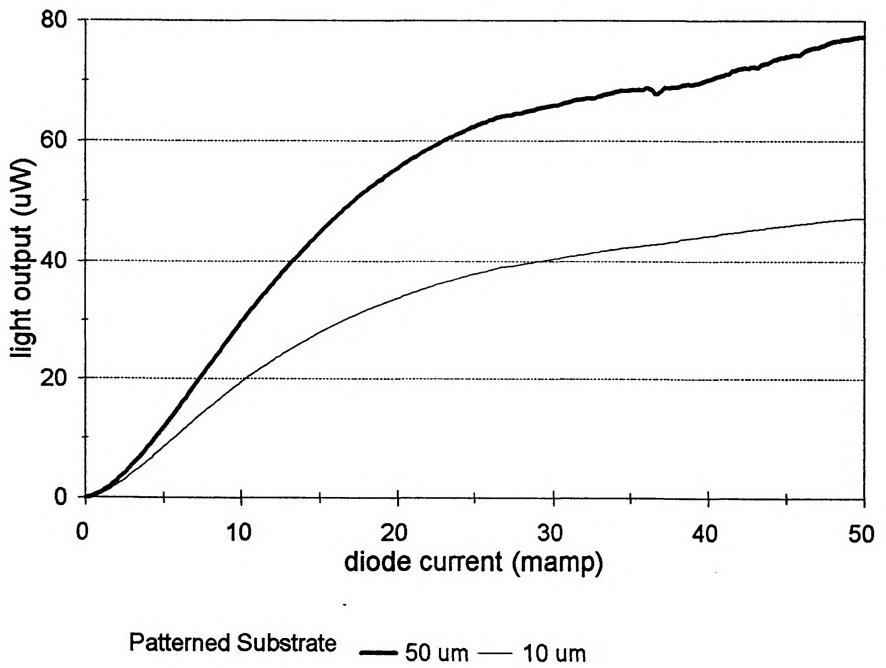

Figure 4.4: *L-I curve of the LED taken at room-temperature with a continuous-wave source. The cavity length is 500 μm.*

4.3.2 Emission Curves

Figure 4.5 illustrates the room-temperature spontaneous emission spectrum. The shift of the peak wavelength is 22 nm (12 meV) with FWHM of 65 nm (36 meV). Photoluminescence measurements on this doped sample (MBE#1255) at 11K reveal a shift of 24 nm; a smaller shift than the 34 nm previously quoted in Chapter 3 for similar growth conditions and slit widths. This could be explained by a slightly lower surface growth temperature, because the substrate was soldered onto a larger wafer for support.

4.4 Discussion

Figure 4.6 illustrates the absorption curves which were calculated from the emission spectrum using the detailed-balance approach of van Roosbroeck and Shockley which gives the equilibrium emission intensity *I(E)* at photon energy *E* as [Casey *et al* 1976]:

$$I(E) \propto \frac{E^2 \alpha(E)}{\exp(\frac{E}{kT}) - 1} \qquad (4.4.1)$$

where $\alpha(E)$ is the absorption coefficient at the energy *E*.

To produce an integrated laser/waveguide device a significant shift must occur so that at the lasing wavelength no light will be absorbed by the waveguide. For this to be the case the laser must be positioned in the region of lower bandgap, corresponding to the narrow stripe region. This optical device requires low defect densities in order to avoid non-radiative transitions. From TEM studies, the interfaces at the centre of 5 μm stripe are dislocation free; however, there are defects at least 1 μm from the edges. The stripe contact style used here, does not seem to have enough lateral confinement to avoid leakage to these defect edges. Therefore, a device with better confinement, such as a ridge or a buried heterostructure, would need to be employed.

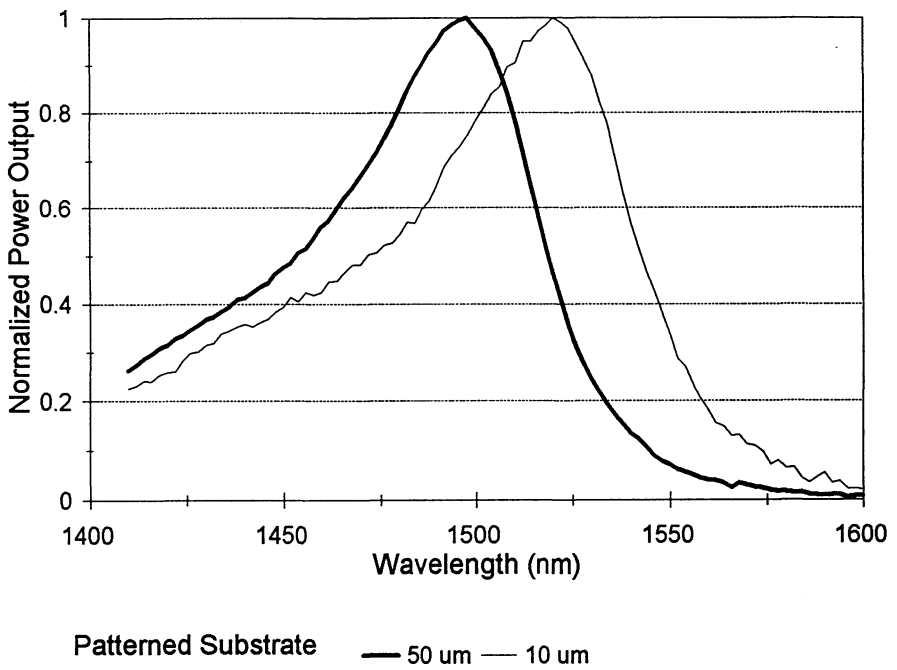

Figure 4.5: *Spontaneous emission spectrum for a LED with a wide (50 μm) and a narrow (10 μm) patterned stripe width. The cavity length is 500 μm.*

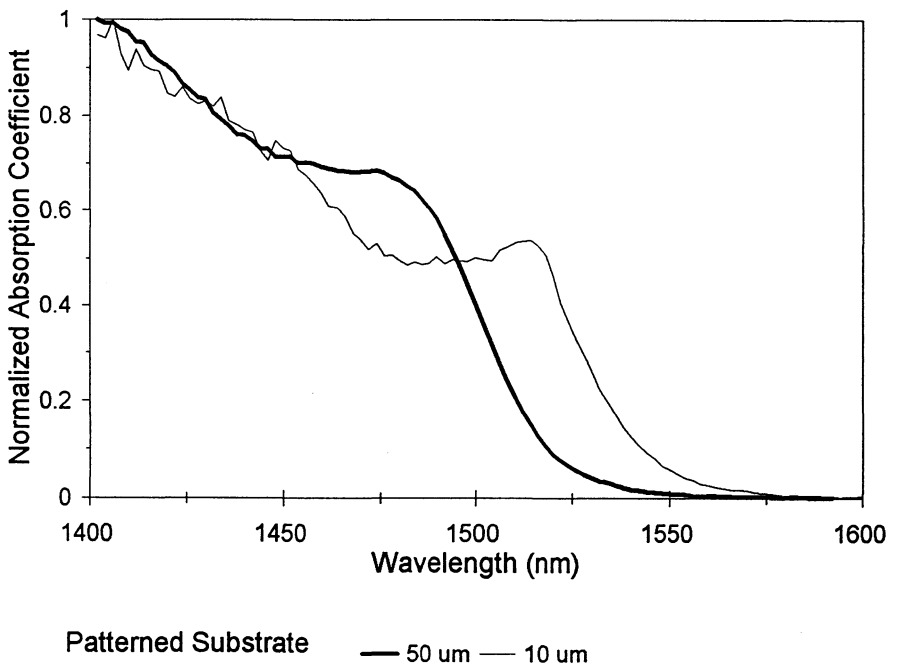

Figure 4.6: *Absorption curve calculated from the spontaneous emission spectrum of figure 4.5.*

The devices produced in this work were edge-emitting LEDs. For a laser produced in this way, the feedback is performed by cleaved facets which set-up a Fabry-Perot cavity. The problem lies in forming cleaved facets when integrating multiple devices. Etched facets have been successfully used to form laser/detector devices [Antreasyan *et al* 1986, Koszi *et al* 1985]; however, this difficulty can be entirely avoided by employing distributed feedback from a Bragg diffraction grating. This has been the focus for much of the work on integrated circuits involving lasers [Aoki *et al* 1986].

CHAPTER 5
CONCLUSIONS

5.1 Summary

Gas source molecular beam epitaxy has been used to grow high-quality InGaAs/InP epitaxial layers in selected areas defined by SiO_2-masked InP substrates. Photoluminescence measurements performed on waveguide stripes which were grown under substrate temperatures ranging from 460 °C to 510 °C and arsine flow rates of 2.2 sccm to 6.1 sccm, revealed that the maximum red-shift occurred when the InGaAs quantum well layer was grown at a high substrate temperature and a low arsine flow rate; both conditions influence the kinetics of growth by increasing the adatom diffusion length. By decreasing the waveguide stripe widths, an increasing red-shift of the peak-wavelength position for the quantum well occurred, suggesting that there exists some continuous control over the entire red-shift range.

A maximum red-shift of 55 nm was measured between a wide stripe width (50 μm) and a narrow stripe width (5 μm). This wavelength shift observed can be partially attributed to a reduction in the quantum-size effect, caused by the incorporation of additional indium and gallium migrating from the masked regions. From TEM measurements, two-thirds of the red-shift can be assigned to the 10-20% thickness increase of the quantum well; however, the observed red-shift cannot be totally accounted for by the thickness change. The calculations performed suggests a 1% increase in the indium composition would be required

to achieve the shifts measured. Although a change in alloy composition due to the relative diffusion coefficients of indium and gallium is expected, no shifts of the bulk PL peak were evident from spectral photoluminescence measurements. As spinodal decomposition was evident in the TEM micrographs, it is possible that the 1% change in composition is overwhelmed by the spinodal excursions. Conversely, scanning PL measurements of the bulk peak wavelength revealed that 20 nm of red-shift occurred upon decreasing the slit width.

The differences in peak red-shift as measured by the spectral PL and scanning PL could be attributed to two systematic factors. First, the scanning photoluminescence system uses a considerably smaller laser spot size; however, the 1 μm diameter is still substantially larger than the compositional modulations of typical dimensions 0.01 μm. Secondly, a red-shift of the low-temperature peak photoluminescence spectra of excitons has been noted on lowering of the excitation intensity, since carriers have the time to migrate to the low-energy sites before recombining [Schubert *et al* 1986]; however, the excitation energy density is approximately 100 times greater for the scanning photoluminescence system. Neither of these factors can explain the discrepancy and further investigations are needed to resolve this issue.

The interfaces in the centre of the stripes were defect free, but stacking faults and faceting occurred at the edges. Mapping of the peak wavelength across the stripe revealed a diffusion profile, with the edges additionally red shifted by 10 nm. Subsequent etching of the edge growth improved the PL results at both room- and low-temperatures.

Finally, a stripe contact light emitting diode was fabricated by the selective-area process. It exhibited a 22 nm shift of the peak spontaneous emission spectrum, which was consistent with the photoluminescence measurements performed.

5.2 Future Work

The results of this work suggest that various paths could be taken to extend the current research. The first recommendation is that the growth conditions governing the red-shift be pushed further by increasing the temperature to 535 °C (since the V/III ratio is already at a minimum of ~1). However, because of the increasing vapour pressure of arsenic with temperature, the group V/III flux ratio may need to be increased to maintain good surface morphologies, and this in turn might reduce the desired increase in migration. Also, at these higher temperatures the lateral composition modulations are enhanced. For a waveguide/laser integrated device, large shifts lead to less absorption losses in the waveguide.

The next recommendation is for a specific LED mask to be designed. This mask should be complete with overlay marks and spacing to allow the pumping of individual devices. A 5 μm width of SiO_2 was found to achieve the largest red-shift associated with the dielectric mask. From PL and TEM investigations, it is clear that defects are generally contained within 1-2 μm of the edge, and a device with better lateral confinement is necessary. Assuming a 5 μm ridge is desired, an allowance of 2 μm on either side of the ridge for edge effects and mask alignment accuracy results in a mask stripe width of 9 μm being suitable.

Since confinement layers are generally InGaAsP, this material system should also be tested since similar shifts were found for InGaAsP as those for InGaAs, when using MOCVD [Joyner *et al* 1992].

APPENDIX

A.1 Photomask layout

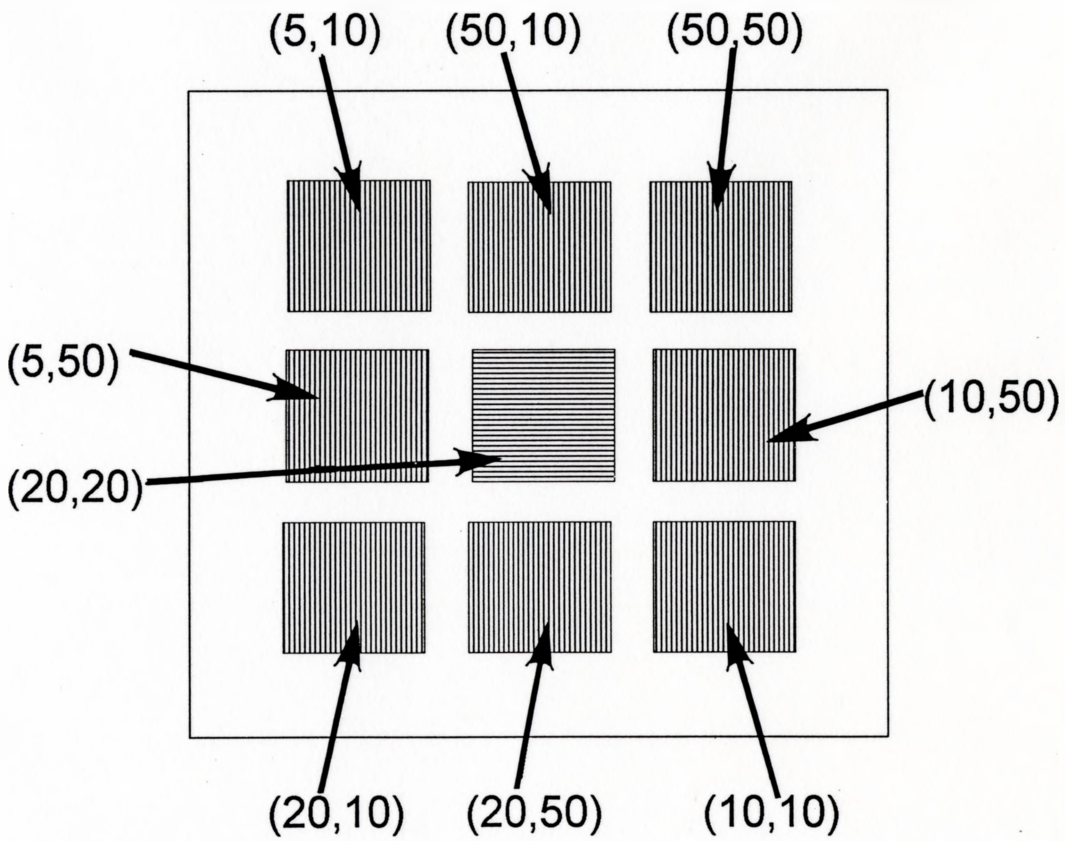

Figure A.1: *Dark field mask definition used to pattern the SiO_2. The dimensions of each square of stripes are (transparent stripe width in µm, opaque stripe width in µm). The overall mask dimensions is 15 mm x 15 mm.*

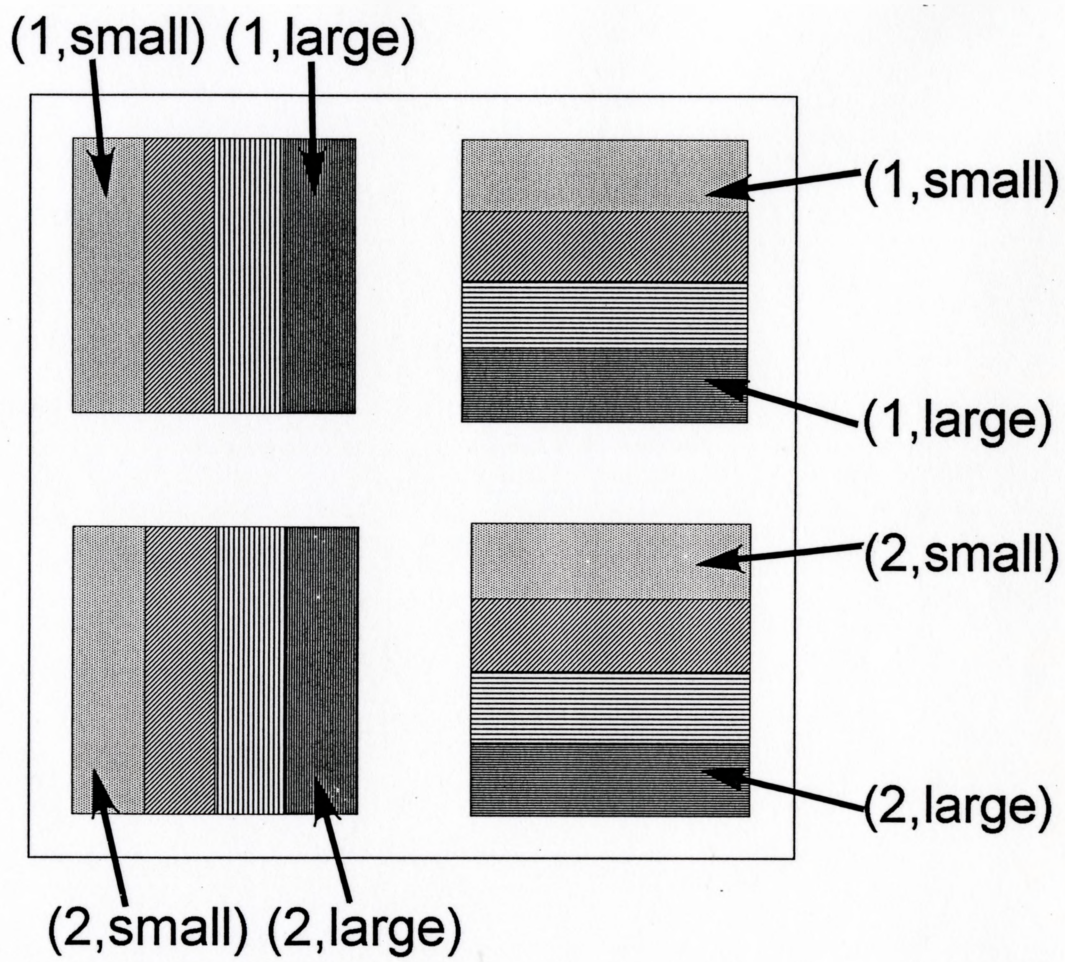

Figure A.2: *Dark field mask definition used to pattern the SiO_2. The dimensions listed on the diagram corresponds to 1 or 2 μm transparent stripes. The opaque stripe widths are 2 μm (small), 4 μm, 7 μm, and 20 μm (large). The overall mask dimension is 15 mm x 15 mm.*

A.2 Compositional Calculations Incorporating Strain

The composition of the bulk ternary $In_{1-x}Ga_xAs$ layer was determined from the equation [Kuphal 1984]:

$$E_g = 0.36 + 0.629\,x + 0.436\,x^2 \qquad \text{(A.2.1)}$$

with E_g taken as PL peak of the room-temperature energy spectrum and $y=1$ (no phosphorous composition). However, this equation is only valid for lattice-matched samples (ie. $In_{0.53}Ga_{0.47}As$). If the composition is different, then the lattice constant of the epilayer no longer matches the InP substrate. Consequently, the lattice constant is extended (if the lattice constant of the epilayer is larger than the lattice constant for InP) or contracted (if the epilayer lattice constant is smaller than that for InP) in the direction normal to the interface as required by the Poisson effect. The elastic tetragonal distortion of the InGaAs lattice does not compromise crystalline quality of an epilayer if the layer thickness is less than the strain dependent critical thickness. In our case, for a 1000 Å $In_{0.53}Ga_{0.47}As$ layer, the mismatch in lattice constants must be less than 0.3% or dislocations will form. This strain induces modifications of the energy band structure which must be taken into consideration when calculating the composition. For example, if the epilayer is indium rich, the alloy layer is under biaxial compression and the conduction-band edge and the "heavy" hole valence-band edge define the bandgap. To first order in strain, the net bandgap shift is [Asai *et al* 1983]:

$$\Delta E = -\alpha\epsilon, \qquad \text{(A.2.2)}$$

where,

$$\alpha = -2a(C_{11} - C_{12})/C_{11} + b(C_{11} + 2C_{12})/C_{11} \qquad \text{(A.2.3)}$$

$$\epsilon = (a_{InP} - a_{epi}) / a_{epi} \qquad \text{(A.2.4)}$$

Here C_{11} and C_{12} are elastic constants; a and b are the hydrostatic and shear deformation

potentials, respectively; ϵ is the strain; and a_{epi} and a_{inP} are the lattice constants of the unstrained epilayer and InP substrate. Since negative strain implies compression, ΔE corresponds to a net bandgap increase. On the other hand, if the epilayer is gallium rich, the alloy layer is in tension and the conduction-band edge and the "light" hole valence-band edge define the band gap. In this case:

$$\alpha = -2a(C_{11} - C_{12})/C_{11} - b(C_{11} + 2C_{12})/C_{11} \qquad \text{(A.2.5)}$$

and since the strain is positive, ie. tension, ΔE corresponds to a net bandgap decrease.

REFERENCES

Aoki M., Suzuki M., Okuno Y., "Multi-Wavelength DFB laser arrays grown by in-plane thickness control epitaxy", Seventh International conference on InP and Related Materials, Japan, pp.53-55 (1995).

Aoki M., Suzuki M., Sano H., Kawano T., Ido T., Taniwatari T., Uomi K., Takai A., "InGaAs/InGaAsP MQW electronabsorption modulator integrated with a DFB laser fabricated by band-gap energy control selective area MOCVD", IEEE J. Quantum Electronics, **29**(5), pp. 2088-2095 (1986).

Arent D.J., Nilsson S., Galeuchet Y.D., Meier H.P., Walter W., "Indium adatom migration during molecular beam epitaxial growth of strained InGaAs/GaAs single quantum wells", Appl. Phys. Lett., **55**, pp. 2611-2613 (1989).

Asai H., Oe K., "Energy Band-gap shift with elastic strain in $Ga_xIn_{(1-x)}P$ epitaxial layers on (001) GaAs substrates", J. Appl. Phys., **54**(4), pp. 2052-2056 (1983).

Bulitka N., V-groove patterned substrate epitaxy using InGaAs/InP, Master's Thesis, McMaster University (1993).

Casey H.C., Stern F., "Concentration-dependent adsorption and spontaneous emission of heavily doped GaAs", J. Appl. Phys., **47**(2), pp. 631-643 (1976).

Chen Y., Zucker J.E., Chiu T.H., Marshall J.L., Jones K.L., "Quantum well electroabsorption modulators at 1.55 μm using single-step selective area chemical beam epitaxial growth", Appl. Phys. Lett., **61**(1), pp. 10-12 (1992).

Cho A.Y., Ballamy W.C., "GaAs planar technology by molecular beam epitaxy", J. Appl. Phys., **46**, pp. 783-785 (1975).

Cotta M.A., Hamm R.A., Staley T.W., Yadvish R.D., Harriott L.R., Temkin H., "Scanning force microscopy measurement of edge growth rate enhancement in selective area epitaxy", Appl. Phys. Lett., **62**(5), pp. 496-498 (1993).

Farrow R.F.C., "Growth of indium phosphide films from In and P_2 beams in ultra-high vacuum", J. Phys. D: Appl. Phys., **7**, pp. L121-125 (1974).

Forrest S.R., Schmidt P.H., Wilson R.B., Kaplan M.L., "Relationship between the conduction-band discontinuities and band-gap differences of InGaAsP/InP heterojunctions", Appl. Phys. Lett., **45**(11), pp. 1199-1201 (1984).

Foxon C.T., Joyce B.A., "Interaction kinetics of As_2 and Ga on {100} GaAs surfaces", Surf. Sci., **50**, pp. 293-322 (1977).

Goodhew P.J., Humphreys F.J., Electron Microscopy and Analysis, Taylor and Francis, London (1988).

Hamm R.A., Faygenson A., Ritter D., Wang Y.L., "Selective area growth of heterostructure bipolar transistors by metal organic molecular beam epitaxy", Appl. Phys. Lett., **61**(5), pp. 592-594 (1992).

Herman M.A., Bimberg D., Christen J., "Heterointerfaces in Quantum Wells and epitaxial growth processes: evaluation by luminescence techniques", J. Appl. Phys., **70**(2), pp. R1-R51 (1991).

Hunsperger R.G., Integrated Optics: Theory and Technology, Springer-Verlag, Berlin (1989).

Joyner C.H., Chandrasekhar S., Sulhoff J.W., Dentai A.G., "Extremely large band gap shifts for MQW structures by selective epitaxy on SiO_2 masked substrates", IEEE Photonics Technology Letters, **4**(9), pp. 1006-1009 (1992).

Kuphal E., "Phase diagrams of InGaAsP, InGaAs and InP lattice-matched to (100) InP", J. Crystal Growth, **67**, pp. 441-457 (1984).

Kuroda N., Sugou S., Sasaki T., Kitamura M., "Selective growth of InGaAs/InP layers by gas source molecular beam epitaxy with atomic hydrogen irradiation", Jpn. J. Appl. Phys., Part 2, **32**(11A), pp. L1627-L1630 (1993).

LaPierre R., Spinodal Decomposition of InGaAsP/InP on (100) and non-(100) Substrates, Master's Thesis, McMaster University (1994).

Okamoto A., "Selective epitaxial growth by molecular beam epitaxy", Semicond. Sci. Technol., **8**, pp. 1011-1015 (1993).

Panish M.B., Temkin H., Gas source molecular beam epitaxy, Springer-Verlag, Germany (1993).

Pratt A.R., Williams R.L., Norman C.E., Fahy M.R., Marinopoulou A., Chatenoud F., "Indium migration control on patterned substrates for optoelectronic device applications", Appl. Phys. Lett., **65**(8), pp. 1009-1011 (1994).

Schubert E.F., Tsang W.T., "Photoluminescence line shape of excitons in alloy semiconductors", Physical Review B, **34**(4), pp. 2991-2994 (1986).

Shibata T., Yamamoto N., Kondo N., Nanishi Y., Fujimoto M., "Effects of ECR-plasma excitation in GaAs MBE growth", Materials Science Forum, **140-142**, pp. 689-704 (1993).

Sze S.M., VLSI technology, McGraw-Hill, New York (1983).

Tanbun-Ek T., Andrekson P.A., Logan R.A., Chu S.N.G., Coblentz D.L., Sergent A.M., Wecht K.W., "DFB lasers with monolithically integrated passive waveguide", IEEE Photonics Technology Lett., **4**(7), pp. 685-688 (1992).

Wang Y.L., Feygenson A., Hamm R.A., Ritter D., Weiner J.S., Temkin H., Panish M.B., "Optical and electrical properties of InP/InGaAs grown selectively on SiO_2-masked InP", Appl. Phys. Lett., **59**(4), pp. 443-445 (1991).

Yamazoe Y., Nishino T., Hamakawa Y., Kariya T., "Bandgap energy of InGaAsP Quaternary Alloy", Jpn. J. Appl. Phys., **19**(8), pp. 1473-1479 (1980).

Yokoyama S., Oogi J., Yui D., Kawabe M., "Low-temperature selective growth of GaAs by alternately supplying molecular beam epitaxy," J. Crystal Growth, **95**, pp. 32-34 (1989).

Zangwill A., Physics at Surfaces, Cambridge University Press, New York (1988).